Advanced Review

Contact-facilitated drug delivery with Sn2 lipase labile prodrugs optimize targeted lipid nanoparticle drug delivery

Dipanjan Pan,[1] Christine T.N. Pham,[2,3] Katherine N. Weilbaecher,[4] Michael H. Tomasson,[4] Samuel A. Wickline[3] and Gregory M. Lanza[3,*]

Sn2 lipase labile phospholipid prodrugs in conjunction with contact-facilitated drug delivery offer an important advancement in Nanomedicine. Many drugs incorporated into nanosystems, targeted or not, are substantially lost during circulation to the target. However, favorably altering the pharmacokinetics and volume of distribution of systemic drug delivery can offer greater efficacy with lower toxicity, leading to new prolonged-release nanoexcipients. However, the concept of achieving Paul Erhlich's inspired vision of a 'magic bullet' to treat disease has been largely unrealized due to unstable nanomedicines, nanosystems achieving low drug delivery to target cells, poor intracellular bioavailability of endocytosed nanoparticle payloads, and the substantial biological barriers of extravascular particle penetration into pathological sites. As shown here, Sn2 phospholipid prodrugs in conjunction with contact-facilitated drug delivery prevent premature drug diffusional loss during circulation and increase target cell bioavailability. The Sn2 phospholipid prodrug approach applies equally well for vascular constrained lipid-encapsulated particles and micelles the size of proteins that penetrate through naturally fenestrated endothelium in the bone marrow or thin-walled venules of an inflamed microcirculation. At one time Nanomedicine was considered a 'Grail Quest' by its loyal opposition and even many in the field adsorbing the pains of a long-learning curve about human biology and particles. However, Nanomedicine with innovations like Sn2 phospholipid prodrugs has finally made 'made the turn' toward meaningful translational success.

How to cite this article:
WIREs Nanomed Nanobiotechnol 2016, 8:85–106. doi: 10.1002/wnan.1355

*Correspondence to: greg.lanza@me.com

[1]Departments of Bioengineering, Materials Science and Engineering, Beckman Institute, University of Illinois, Urbana-Champaign, IL, USA

[2]Division of Rheumatology, Department of Medicine, Washington University School of Medicine, St. Louis, MO, USA

[3]Division of Cardiology, Department of Medicine, Washington University School of Medicine, St. Louis, MO, USA

[4]Division of Oncology, Department of Medicine, Washington University Medical School, St. Louis, MO, USA

Conflict of interest: The authors have declared no conflicts of interest for this article.

The copyright line for this article was changed on 05 October 2015 after original online publication.

INTRODUCTION

Nanomedicine offers approaches to recalcitrant medical problems by providing tools to detect and characterize pathology based on the unique expression of cell surface biosignatures as well as to deliver therapeutic compounds more specifically to such lesions using the same platform technology, i.e., so called theranostic agents. Among the more effective class of theranostic agents reported to date are the lipid-based particles, including liposomes, micelles, and emulsions. Their success has been derived from an

inherently high biocompatibility associated with phospholipids, a general ease of lipid functionalization, and their 'soft' compliant three-dimensional (3D) morphology.

Therapeutic compounds are easily incorporated into lipid-based particles (i.e., liposomes, micelles, or emulsions) within the membranes or core, which may be aqueous or 'oil' or even lipophiles. A well-known nontargeted example is Doxil™, a pegylated liposomal formulation.[1] Doxil elimination follows a typical bi-exponential curve characterized by a rapid distribution phase with a 2-h half-life and a much slower beta-elimination rate (45 h $t_{1/2}$). Incorporation of the Adriamycin into the aqueous phase of liposomes decreased the volume of distribution in patients to 4 L from 254 L for free drug.[1] The constrained volume of distribution and extended circulatory half-life markedly improved the efficacy of doxorubicin over free drug. Abraxane, a nontargeted paclitaxel emulsion nanoparticle, improved the clinical effectiveness of paclitaxel over the original Cremophor EL formulation by allowing more rapid infusion rates without premedication and by increasing the maximum tolerated dose.[2] Clearly, particulate encapsulation of drugs can provide unique attributes that improve clinical utility.

The success of Doxil, the advent of monoclonal antibody technology, and Paul Erhlich's, Nobel laureate 1908, inspired vision of a 'magic bullet' to treat disease fueled the era of targeted drug delivery based on particles that continues robustly today. However, it was soon recognized that the internalization of therapeutic compounds through ligand (antibody)-targeted particles generally passed through an endosomal compartment, which diminished the effectiveness of the drug in comparison to the same exposure of free drug to the cell surface.[3] Subsequently, investigators probed innumerable approaches to overcome endosomal-related losses of therapeutic cargoes of drugs, oligonucleotides, and proteins. Cationic cell-penetrating peptides, such as Tat (transactivator of transcription) were studied as a mechanism to enhance intracellular delivery.[4] However, these cationic peptides interact with cell-associated glycosaminoglycans and payloads are subsequently internalized by and lost to endocytosis. Arginine-rich CPPs coupled directly to peptide nucleic acids (PNA) or phosphorodiamidate morpholino oligomers (PMO) have found improvement at noncytotoxic doses without endosomolytic agents,[4] but the same is not found for cationic nanoparticles.[5] In the context of siRNA and gene delivery, effective delivery of the nucleic acid-based therapy from endosomes to the nucleus has received considerable scientific attention with some promising successes.[6–25]

Contact-Facilitated Drug Delivery

In contradistinction to the investigators seeking to internalize particles into cells for drug delivery, we have pursued a novel approach to targeted drug delivery and termed it 'contact-facilitated drug delivery' (CFDD).[26] CFDD refers to the transfer of bound nanoparticle lipid surfactant components into the outer leaflet of the target cell membrane. This is a slow second-order process dependent upon the persistent interaction of the nanoparticle with target membrane surfaces. Casual interactions of lipid encapsulated nanoparticles in circulation with other cell surfaces have no significant consequence noted to date. Figure 1 illustrates the transfer of rhodamine-coupled phosphatidylethanolamine, a membrane marker, to the outer and inner membranes of a C32 cell in culture.[27] Close examination (inset) shows the literal streaming of the fluorescent phospholipid onto the cell surface. Electron microscopic examination captured the hemifusion complexation of the monolayer of a perfluorocarbon (PFC) nanoparticle (~250nm) with

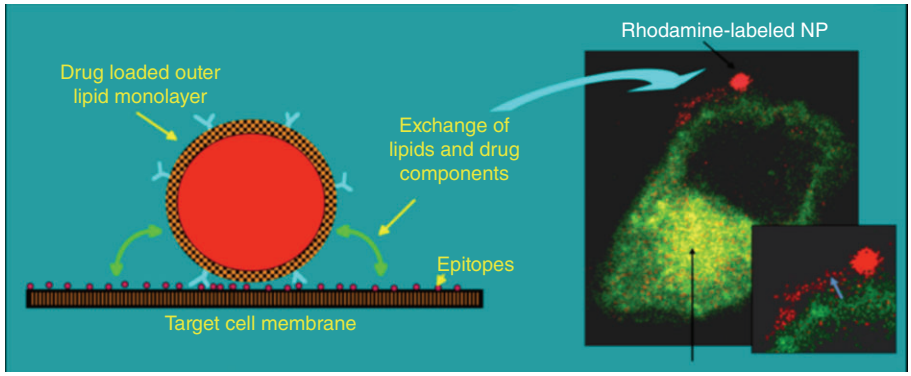

FIGURE 1 | Contact-facilitated drug delivery illustrated with rhodamine PFOB nanoparticle bound to C32 melanoma cell (transfected with Rab GFP endocytic markers). (Reprinted with permission from Refs 26 and 27. Copyright 2002 and 2008)

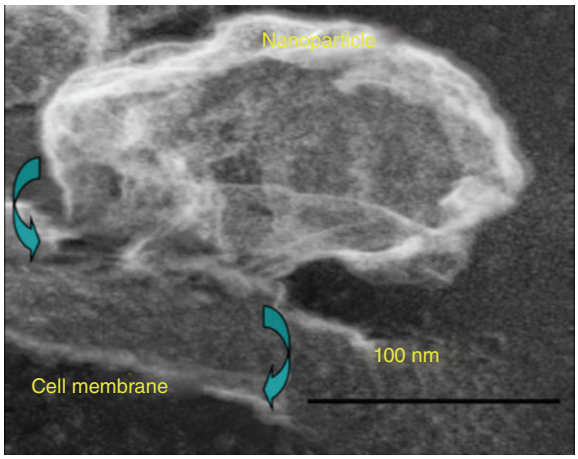

FIGURE 2 | SEM showing PFOB nanoparticle hemifusion complex to C32 melanoma cell. (Reprinted with permission from Ref 28. Copyright 2009)

the bilayer of target cell membrane (Figure 2).[28] In effect, theranostic nanoparticles deliver a 'kiss of death' without the requisite cellular internalization of the nanoparticles or escape of the drug payload from an endosomal compartment.

CFDD proved effective *in vivo* for delivery of antiangiogenic drugs, particularly fumagillin in combination with MR angiogenesis imaging using $\alpha_v\beta_3$-targeted PFC nanoparticles. For example, in the Vx2 syngeneic adenocarcinoma tumor model $\alpha_v\beta_3$-targeted PFC nanoparticles delivering native fumagillin (0.049mg/kg) in three serial minute doses, greater than 10,000-fold reduction in the systemic TNP-470 dose, a water soluble analogue, used in human clinical studies dramatically reduced tumor development and angiogenesis, which was clearly revealed by 3D reconstruction of the tumors and their angiogenic maps created with the same platform technology (Figure 3(a)).[29] Similarly, in hyperlipidemic NZW rabbits with early aortic atherosclerosis, $\alpha_v\beta_3$-targeted nanoparticles provided an MR-based estimate of the overall plaque burden as reflected by expanded neovascularity, delivered effective fumagillin antiangiogenic therapy, and provided quantitative follow-up of treatment response (Figure 3(b)).[30] More recently, in the K/BxN mouse model of inflammatory arthritis, which expresses the T-cell receptor transgene KRN and the MHC class II molecule A(g7), $\alpha_v\beta_3$-targeted fumagillin nanoparticles administered serially decreased arthritic score, ankle thickness, inflammation, proteoglycan depletion, and angiogenesis (Figure 3(c)).[31] In each example, the dose of fumagillin was well below the serial dosages of TNP-470 (30 mg to 60 mg/kg), used in similar applications. Importantly, TNP-470 at therapeutic doses, particularly in cancer patients, was associated with neurocognitive deficits,[32–34] which could be eliminated by targeted nanotherapy.

However, closer examination of these preclinical Nanomedicine results indicated that increased dosages, both in terms of drug payload per particle and drug dose per animal, were required as the pathologic intensity of the disease model increased. Moreover, other hydrophobic membrane dissolved drugs, such as paclitaxel, were rapidly lost from the PFC nanoparticle surfactant *in vivo* despite being very

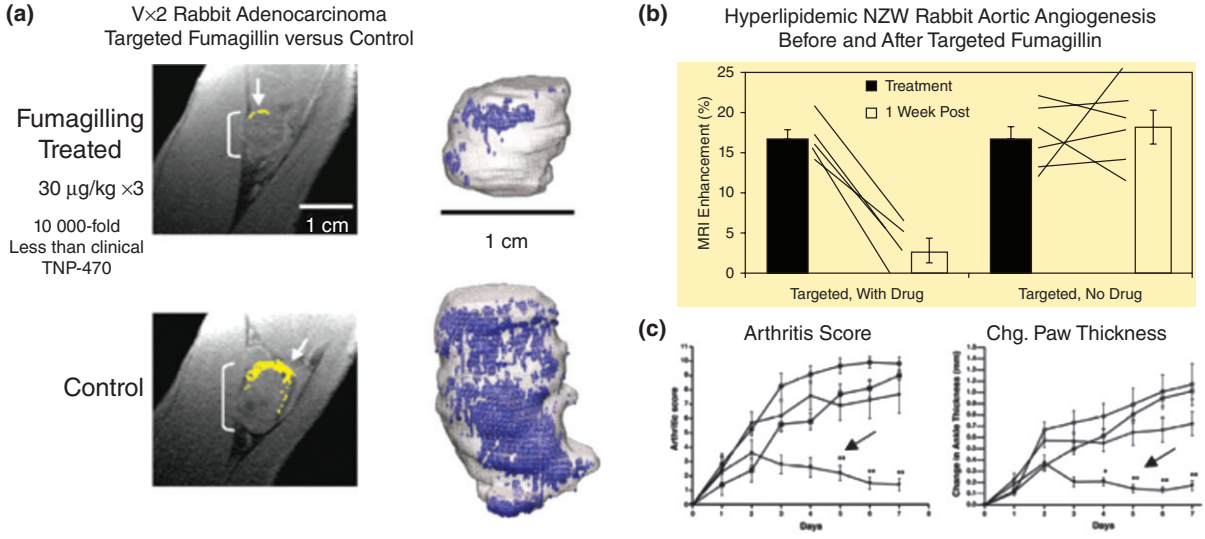

FIGURE 3 | (a) Three-dimensional MR angiogenesis maps of control and integrin-targeted fumagillin NP in Vx2 model. (b) Angiogenesis contrast before and 1 week after a fumagillin or control NPs in hyperlipidemic rabbits. (c) Decreased arthritic score and ankle thickness following targeted fumagillin in the K/BxN model of inflammatory arthritis. (Reprinted with permission from Refs 29–31. Copyright 2008, 2006, and 2009)

stable in the vial with limited release during *in vitro* dissolution studies.[26] *In vivo* pharmacokinetic studies simultaneously tracking the perfluorocarbon (PFC) core, the lipid-conjugated peptidomimetic homing ligand, and a lipid-conjugated paramagnetic chelate in rodents showed that the lipid anchored-chelate and integrin homing ligand tracked closely with the clearance of PFC from the blood, indicating that these components of the nanoparticles were intact. However, fumagillin[35] or paclitaxel (unpublished) dissolved into the membranes cleared much faster than the PFC, indicating their rapid premature diffusion from the particle surface into the plasma and extravascular space.

An initial approach to overcome this problem was to couple drugs, such as paclitaxel, to the amine of phosphatidylethanolamine, analogous to the peptidomimetic homing ligand and paramagnetic chelate, using esterase labile intervening linkages of different length. In a series of unpublished experiments, these paclitaxel prodrugs incorporated stably into the nanoparticle surfactant membrane and were stable in circulation, but intracellular bioavailability of the drug was ineffective after binding to the target *in vitro* and *in vivo*. In hindsight, this poor result could have been anticipated, since we previously noted poor cellular internalization of compounds with large phospholipid head group modifications, such as paramagnetic DOTA-chelates that were used to impart r1 relaxivity for molecular imaging. Gadolinium mass balance studies showed that the lanthanide-chelate complex was liberated rapidly from the lipid anchor, likely by phospholipase D, and bioeliminated through urine. Although the use of exogenous energy, such as ultrasound, could be applied to force these compounds and particles into the cell endosomal compartment,[27] the preferred approach to drug delivery remained the 'contact facilitated mechanism'.

The concept of a phospholipid prodrug was considered as a novel means to couple the active pharmaceutical ingredient (API) through the Sn2 acyl position (i.e., stereospecific numbered hydroxyl group of the second carbon of glycerol) and retain the advantages of CFDD. This compound could stably self-assemble into the phospholipid surfactant membrane of particles positioning the drug in a protective hydrophobic environment during circulatory transit to the target site. Once docked to a cell surface receptor, contact-mediated streaming of the phospholipid prodrug into the outer leaflet of the target cell membrane would be facilitated. Translation of the lipid-prodrug from the outer lipid leaflet into the inner lipid leaflet would encourage rapid distribution of the prodrug throughout the intracellular membranes and active drug liberation by target cell phospholipase(s).

PHOSPHOLIPID SN2 PRODRUGS WITH LIPOSOMES

Phospholipases A2 (PLA_2) is part of a super family of enzymes that catalyze the hydrolysis of the Sn2 ester bond in a variety of phospholipids releasing a free fatty acid and a lysophospholipid. These enzymes are classified as five major types: secreted low molecular weight $sPLA_2$s, larger cytosolic Ca^{2+}-dependent $cPLA_2$s, Ca^{2+}-independent $iPLA_2$s, platelet-activating factor (PAF) acetylhydrolases, and lysosomal PLA_2s.[36] The hydrolysis of the Sn2 ester bond represents the first step in a pathway to many second messengers, e.g., the conversion of liberated arachadonic acid into eicosanoids, which exert a wide range of physiological and pathological effects. In endothelial cells, multiple family members of different types of phospholipases are present thereby creating a rich repertoire of potential activating agents within target cells. Moreover, beyond these known types of lipases in endothelial cells, additional serine hydrolases (or other hydrolases) are present, which could also hydrolyze prodrug to active drug in target cells.

Although the concept of Sn2 phospholipid prodrugs had never been considered for targeted drug delivery associated with CFDD, precedence for the formation of Sn2 phospholipid prodrugs was initially reported by David Thompson et al.[37] in the context of triggered release mechanisms. Later Thomas Lars Andresen and colleagues[38–48] pursued an approach to deliver chemotherapeutics as Sn2 prodrugs via untargeted liposomes. They anticipated that increased liberation of phospholipases by cancers would trigger release of the compounds in the proximity of a tumor increasing the local drug bioavailability. The effectiveness of this approach was modest and further enhancement by utilizing a thermosensitive untargeted prodrug liposome with exogenous heating was only marginally better.[38] Importantly, these investigators noted that nonpegylated liposomes, which are highly susceptible to intravascular clearance and destruction, were more resistant to PLA2 drug liberation than the more commonly used stealth or pegylated liposomes. Their data suggested that pegylation of liposomes to extend intravascular circulation undesirably predisposed the vesicles to premature drug release by PLA2. They further showed that the efficacy of the liposomal Sn2 prodrugs to liberation by secretory phospholipases was dependent on water accessibility to the bond, which was less available for the synthetic ether-lipid prodrugs than for natural lipids. Pegylation enhanced water penetration and enzyme access to the bond. Targeted PFC nanoparticles or nanoemulsions and other lipid micelle particles to be discussed subsequently were adequately stable *in vivo* without

pegylation. The reduced water accessibility of the Sn2 prodrug was highly desirable for preventing premature release or metabolism until the ligand-mediated binding to the target cell and CFDD ensued.

Other investigators considered phospholipid prodrugs for improved oral delivery of indomethacin and valproic acid.[49,50] In those studies, Sn2 phospholipid conjugates were utilized to affect oral controlled release of drugs by continuous degradation of the phospholipid prodrug within the intestine. Unfortunately, oral administration of the indomethacin Sn2 prodrug decreased the total amount of drug absorbed in comparison to the administration of free indomethacin, although it smoothed the plasma concentration versus time profile curve, delayed T_{max} and lowered $C_{max.}$[50] Intravenous administration of the prodrug in untargeted liposomes further reduced the bioavailability of the APIs relative to oral administration of the phospholipid prodrug or the free drug. Importantly, direct attachment of indomethacin to the Sn2 ester completely blocked PLA_2 hydrolysis activity, while insertion of short spacers between the drug and the ester bond greatly improved activity.

Mitomycin C, an antibiotic and broad-spectrum cytotoxic agent, with a notoriously narrow therapeutic window, was studied as a lipophilic prodrug for use in pegylated liposomes.[51–53] In contradistinction to the Sn2 ester linkage pursued by others, the drug was coupled through a disulfide bond that remained stable within circulating pegylated liposomes. This approach takes advantage of an abundance of reducing agents within tumors and their microstroma to liberate the API. Mitomycin-C prodrug liposomes had reduced toxicity and superior efficacy when compared to free mitomycin C in ectopic rodent xenograft tumor models. The prodrug liposomes were more effective than chemotherapeutic comparators, including irinotecan and gemcitabine, in gastrointestinal and pancreatic rodent models. As expected, these liposomal drug formulations had virtually complete prodrug incorporation into the lipid bilayer membranes during synthesis within which, the sensitive API remained chemically protected.

SN2 PHOSPHOLIPID PRODRUGS AND CFDD

Fumagillin

As reported by others, fumagillin is an antiangiogenic agent specific for proliferating endothelial cells. Fumagillin can inhibit the formation of angiogenic vessels by inhibiting methionine aminopeptidase. Although fumagillin was isolated from the fungal organism Aspergillus fumigatus, its water soluble clinical analog, TNP-470 was produced semi synthetically. TNP-470 was found to be effective in rodents but possessed only anecdotal effectiveness in the clinic at the high doses required. At clinical dosages, TNP-470 was associated with numerous toxicities, including neurocognitive dysfunction.[34,54,55] Fumagillin, incorporated into the phospholipid surfactant of nanoparticles for targeted antiangiogenesis therapy, can be used at a much lower and safer dosages.[29,30,56]

Despite promising *in vivo* results, the 'drugability' of native fumagillin is inherently compromised by photochemical instability associated with a conjugated decatetraenedioic tail, which is known to undergo rapid degradation even in day light. Furthermore, the presence of two chemically reactive epoxide rings at the active site makes this compound highly vulnerable towards an acidic environment, light and other drastic conditions. Pharmacokinetic studies demonstrated that hydrophobic drugs, such as fumagillin, stably incorporated into the phospholipid surfactant of perfluorocarbon nanoparticles during dissolution studies were rapidly lost and likely metabolized during particle circulation *in vivo*.[35] To address this, an Sn2 fumagillin prodrug (Fum-PD) was envisioned and the compound was synthesized in a straightforward way in two-steps involving saponification of fumagillin dicyclohexylamine salt to fumagillol and a subsequent esterification with oxidized lipid 1-palmitoyl-2-azelaoyl-sn-glycero-3-phosphocholine (PAzPC) (Figure 4).[35]

Recently, the antiangiogenesis efficacy of $\alpha_v\beta_3$-Fum-PD nanoparticles was visualized *in vivo* using a novel phospholipid-encapsulated copper oleate in oil nanoparticle (CuNP) and photoacoustic microscopic imaging (PA) of neovasculature formed in a subcutaneous Matrigel™ rodent model.[57] Mice implanted with Matrigel™ 18 days previously received $\alpha_v\beta_3$-CuNPs, nontargeted CuNPs, or $\alpha_v\beta_3$-CuNP preceded by 10 min with a competitive dose $\alpha_v\beta_3$-oil only NPs (1:1). As seen in Figure 5, at 0 min, forming vascular tubules were observed by the inherent PA contrast imparted by erythrocyte hemoglobin. Following $\alpha_v\beta_3$-CuNP injection, numerous incomplete vascular sprout offshoots largely devoid of erythrocytes were noted. These sprouts were previously characterized to be nonpolarized immature endothelial cells ($\alpha_v\beta_3^+$, Tie-2$^-$, and CD31$^+$) as opposed to formed microvessels with polarized endothelium, which were $\alpha_v\beta_3^-$, Tie-2$^+$, and CD31$^+$.[58] The formation of the angiogenic shoots depicted an early evolution stage of a dense and irregular neovasculature. Animals given nontargeted-CuNPs had very little change in PA signal with minimal passive

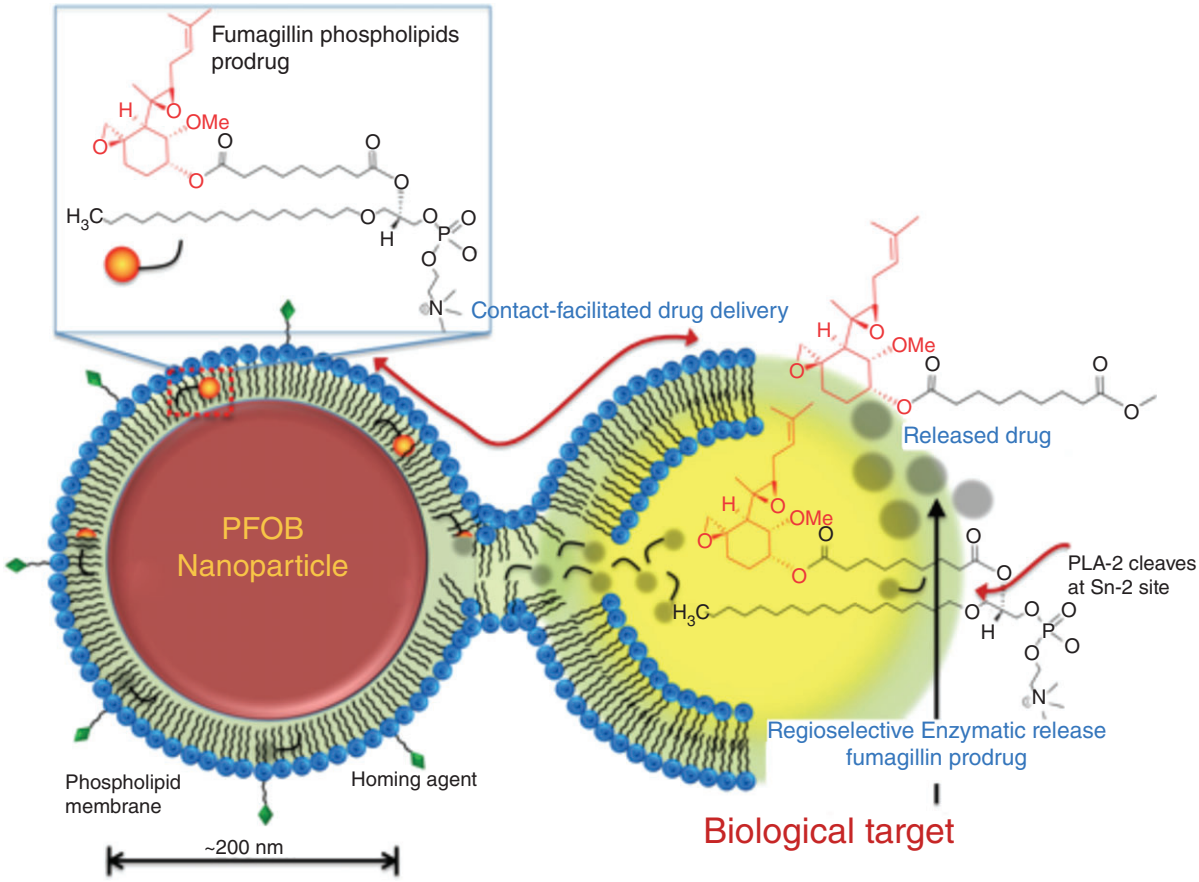

FIGURE 4 | Schematic representation of contact-facilitated drug delivery mechanism with Sn2 lipase labile fumagillin prodrug inserted into the lipid membrane of a PFC nanoparticle. Ligand tethering of the nanoparticle to the target cell support the formation of a hemifusion complex between the two membrane surfaces. Translation of the Fum-PD into the inner leaflet of the target cell membrane leads to its distribution through the cell except the mitochondria. Regioselective enzymatic cleavage at the Sn2 site by phospholipase (such as phospholipase A2, PLA2) liberates the drug into the cytosol. (Reprinted with permission from Ref 63. Copyright 2012)

accumulation affording slight blood pool enhancement. In the competition group, very little change in the PA signal from the vascular tubules or sprouts was observed. Pretreatment with $\alpha_v\beta_3$-targeted NPs comprising oil core (no Cu oleate) blocked the receptors to $\alpha_v\beta_3$-CuNP binding and even precluded significant passive blood pool accumulation.

$\alpha_v\beta_3$-CuNPs incorporating Fum-PD within the phospholipid membrane were administered on days 11 and 15 post Matrigel™ implant. At baseline on day 18, the amount of neovasculature observed by PA imaging was sparse, similar to that observed in the other groups. Following $\alpha_v\beta_3$-CuNP injection, there was negligible sprout enhancement at 170 min. Blood vessel PA signal was similar to that measured in the nontargeted CuNP group. 'Pruning' of neovasculature was first suggested by Dr. Rakesh Jain in a visionary manner; but in this study, the concept was visually apparent with Fum-PD and PA microscopic imaging.[59–61]

$\alpha_v\beta_3$-Fum-PD Nanoparticles Suppress Inflammation in the KRN Model of Arthritis

In the K/BxN model of inflammatory arthritis, passive transfer of K/BxN serum into mice is used to induce a polyarticular inflammatory arthritis resembling rheumatoid arthritis (RA).[62] Using this model, serial i.v. injections of $\alpha_v\beta_3$-Fum-PD NP after K/BxN serum transfer, in mice with clearly established arthritis, significantly attenuated disease progression at doses eightfold lower than that previously reported using native fumagillin (0.3 mg/kg vs 2.4 mg/kg).[31,63] By contrast, inflammation progressed rapidly and unabated in the group of mice that received $\alpha_v\beta_3$-Ctrl NP (Figure 6). In addition to clinical scores, histologic examination of arthritic paws revealed that $\alpha_v\beta_3$-Fum-PD NP limited inflammatory leukocyte recruitment to the inflamed paws and protected against bone erosions and cartilage damage (Figure 6). More importantly, joint-associated inflammatory biomarkers VCAM-1 and ICAM-1 and the

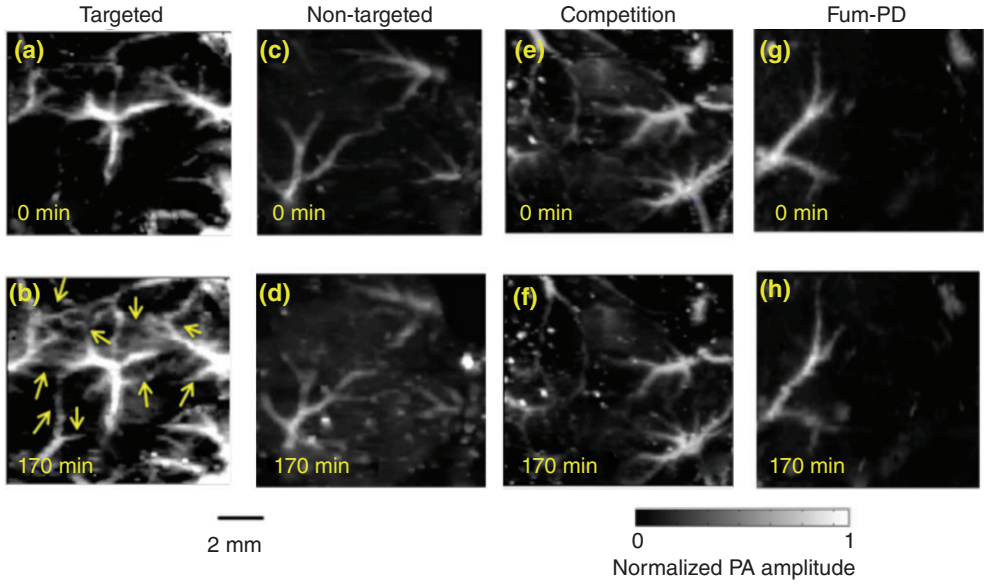

FIGURE 5 | *In vivo* PA images of the Matrigel™ plug area implanted in four groups of mice at 18 days using $\alpha_v\beta_3$-CuNPs. (a, b) Targeted CuNPs group. The enhanced neovasculature by Cu Oleate NPs are marked by arrows in (b). (c, d): Nontargeted CuNPs group. (e, f) Competition group: mice received a competitive dose $\alpha_v\beta_3$-oil only NP (1:1) 10 min before $\alpha_v\beta_3$-CuNPs. (g, h) Fum-PD group: mice received $\alpha_v\beta_3$-CuNPs with Fum-PD 11 and 15 days after the Matrigel™ implantation then $\alpha_v\beta_3$-CuNPs w/o fum-PD on day 18 for PA imaging. For all PA images, laser wavelength = 767 nm. (Reprinted with permission from Ref 57. Copyright 2015)

major pro-inflammatory cytokines and chemokines (IL-1β, IL-6, MCP-1, and TNF-α) were all diminished with $\alpha_v\beta_3$-Fum-PD NP treatment relative control NP injections. While fumagillin is well known to impact the proliferation of neovascular endothelial cells, the direct impact of this mycotoxin on nonendothelial cell types is negligible.[64,65]

Follow-up studies presented evidence that Fum-PD nanotherapy indirectly suppresses inflammation in K/BxN arthritis through the local production of endothelial nitric oxide (NO). Fum-PD-induced NO modulated macrophage inflammatory response through AMP-activated protein kinase (AMPK). NO-induced AMPK activation decreased mammalian target of rapamycin (mTOR) activity and increased autophagic flux, as evidenced by p62 depletion and increased autolysosome formation *in vivo*. Increased macrophage autophagy flux was associated with degradation of IkappaB kinase (IKK), suppression NF-κB-p65 signaling pathway and ultimately decreased inflammatory cytokine release.[66]

$\alpha_v\beta_3$-Fum-PD NP Therapy Enhances the Effectiveness of Methotrexate

Methotrexate (MTX) is commonly used to treat rheumatoid arthritis (RA) but the onset of clinical benefit is delayed by weeks and the therapeutic response is seldom complete. We have previously demonstrated that native fumagillin NP in combination with MTX led to significantly improved and sustained response that could not be achieved with either agent alone.[67] To corroborate this finding, a combination $\alpha_v\beta_3$-Fum-PD NP and MTX was administered to mice using the K/BxN serum transfer model. $\alpha_v\beta_3$-Fum-PD NP was given as single treatment (x1) on day 2 after K/BxN serum transfer and MTX was given on days 3, 5, and 7. The combination of $\alpha_v\beta_3$-Fum-PD NP (1X) + MTX produced a 55% reduction in clinical disease indices by day 9. Of note, the combination of $\alpha_v\beta_3$-Fum-PD NP given twice (on days 2 and 4) + MTX (on days 3, 5, and 7) led to further improvement in disease activity (~60% sustained reduction) over the 9-day study (data not shown). The improvements in disease activities with the combination $\alpha_v\beta_3$-Fum-PD NP (x1) + MTX were greater than the responses observed with $\alpha_v\beta_3$-Ctrl NP + MTX while treatment with $\alpha_v\beta_3$-Fum-PD NP (x1) without MTX did not lead to sustained clinical response. Mice treated with the combination of $\alpha_v\beta_3$-Fum-PD NP + MTX also lost less body weight during the study and rebounded to pretreatment weight by day 9, while the weight loss among animals in all other experimental groups remained below baseline. The combination of $\alpha_v\beta_3$-Fum-PD NP + MTX suppressed the influx of inflammatory cells into arthritic paws by approximately 90%, which was an additional 30% reduction in inflammatory leukocytes recruitment seen in the $\alpha_v\beta_3$-Ctrl NP + MTX group. Dual $\alpha_v\beta_3$-Fum-PD

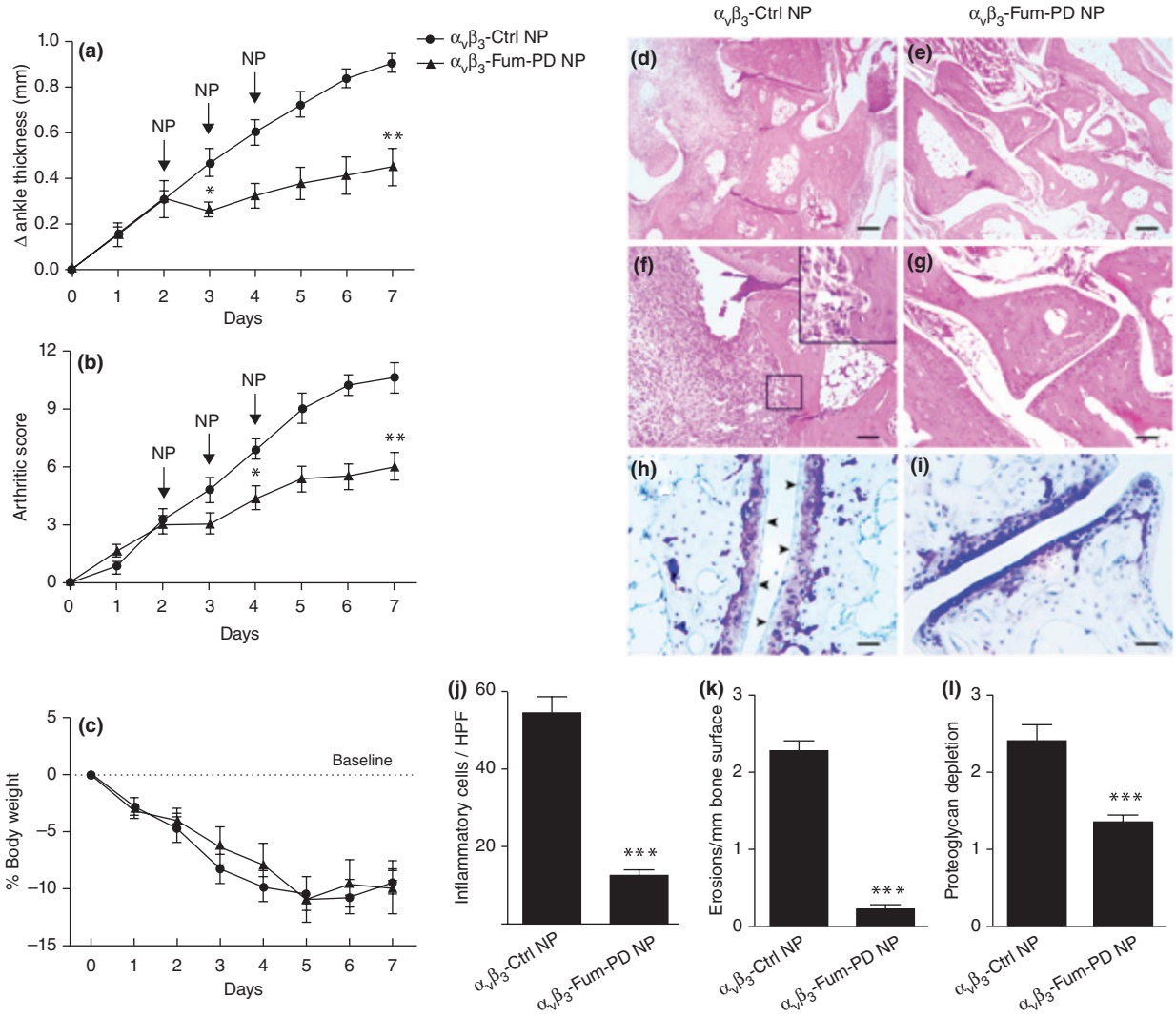

FIGURE 6 | $\alpha_v\beta_3$-Fum-PD NP suppressed inflammatory arthritis in the KRN model. Targeted particle with and without drug were administered on days 2, 3, and 4 (arrows). Changes in ankle thickness (a), arthritic score (b), and body weight (c) were monitored daily. Histology on day 7 for inflammatory cell number per high power field (HPF; d, e, j), erosions (f, g, k), and proteoglycan depletion (h, i, l) $^{*}P < 0.05$, $^{**}P < 0.01$, $^{***}P < 0.0001$. (Reprinted with permission from Ref 63. Copyright 2012)

NP-MTX therapy was also superior to other treatments in preventing bone erosions and in preserving cartilage integrity (Figure 7).

These experiments revealed that the lipase-labile Sn2 Fum-PD was bioequivalent to native fumagillin when incorporated into integrin-targeted PFC nanoparticles along with improved photochemical stability and nanoparticle surfactant retention. Antiangiogenic therapies are typically used as adjuvant therapies for acute benefit to accelerate or enhance the efficacy of a primary therapy. In this series of experiments, single dose $\alpha_v\beta_3$-Fum-PD NP significantly enhanced the efficacy of MTX.

While fumagillin is an established antiangiogenic compound, other drugs, such as taxanes used at lower dosages also have potent antiangiogenesis properties. A brief pilot study testing a lipase-labile Sn2 paclitaxel prodrug given serially (on days 2, 3, and 4), analogous to previous Fum-PD NP studies,[63] demonstrated markedly improved effectiveness against arthritis manifestation in the K/BxN model, virtually suppressing all clinical indices during this entire study interval (Figure 8). These results were followed by further evaluation of $\alpha_v\beta_3$-docetaxel-prodrug in the very aggressive Vx2 rabbit squamous carcinoma model.

Docetaxel

Despite extensive clinical research on the effects and benefits of antiangiogenesis therapy in cancer and

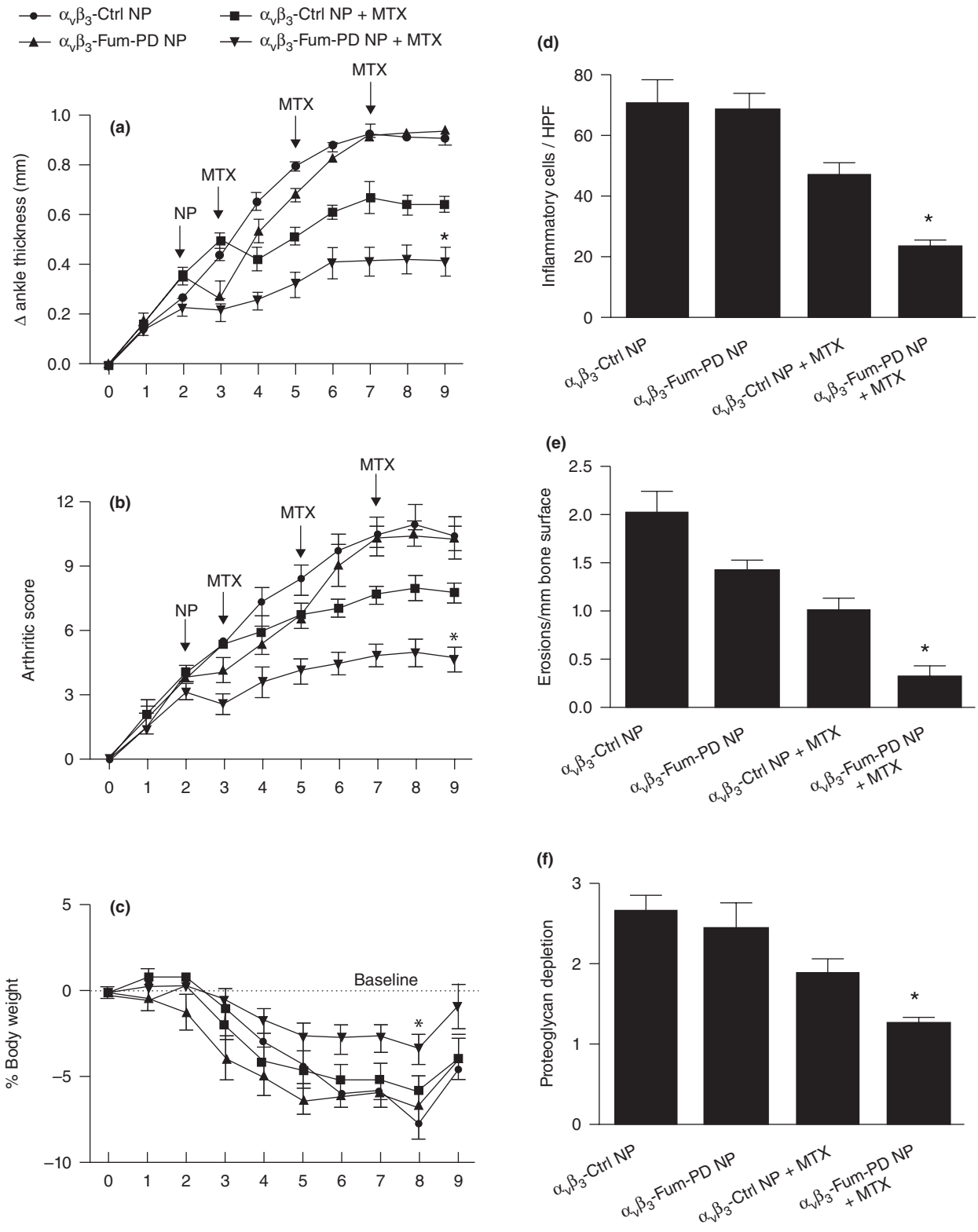

FIGURE 7 | $\alpha_v\beta_3$-Fum-PD NP (1X) in combination with MTX suppressed inflammatory arthritis in the KRN mouse model. $\alpha_v\beta_3$-Fum-PD NP or $\alpha_v\beta_3$-control NP were given on day 2 ($n = 5$/group) and changes in ankle thickness (a) arthritic score (b) and body weight (c) were monitored daily. Histology on day 9 revealed significant benefit for inflammatory cell number/HPF (d), erosions (e), and proteoglycan depletion (f).* $P < 0.05$.

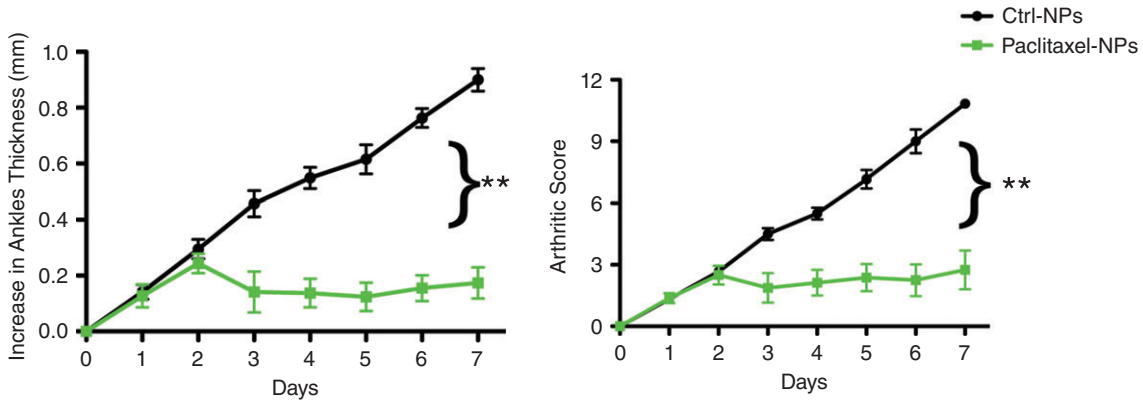

FIGURE 8 | $\alpha_v\beta_3$-Paclitaxel-PD NP suppressed inflammatory arthritis in the KRN model. Targeted particle with and without drug were administered on days 2, 3, and 4 (arrows). Changes in ankle thickness (a) and arthritic score (b) were monitored daily ** $P < 0.01$.

selected other pathologies, virtually all of the work has centered on vascular endothelial growth factor (VEGF) inhibition. While VEGF is a clear driver of angiogenesis, it elicits pleotropic effects and is not solely responsible for neovascularization.[68] Moreover, VEGF is produced by a variety of cell types, making effective blockade of the growth factor challenging. Typically, relatively high dosages of medicants are used clinically and these treatments have well known side effects.[69]

Paclitaxel is a cytoskeletal drug that interacts with tubulin to corrupt mitotic spindle assembly, chromosome segregation, and cell division by inhibiting microtubule disassembly. As a consequence, chromosomes are unable to achieve proper metaphase configuration and mitotic progression is blocked. The inability to complete cell division promotes apoptosis or reversion to a quiescent G_0-phase of the cell cycle. The rarity of paclitaxel, initially isolated from the Pacific yew, led to synthetic chemical pathway development and the emergence of docetaxel, a close chemical analog of the index compound with similar biological properties. Taxanes have found clinical applications as a cytotoxic cancer chemotherapeutic[70] as well as stent-delivered inhibitors of restenosis following angioplasty.[71] In Nanomedicine, the hydrophobic nature of paclitaxel has favored its incorporation into many nanoparticle formulations, including into the phospholipid outer membrane of PFC nanoparticles.

Lipid-encapsulated perfluorocarbon nanoparticles have been targeted to a myriad of epitopes for diagnostic imaging and site-specific drug delivery for applications in atherosclerosis, restenosis, cancer, and RA.[31,67,72,73] Preliminary studies in the Vx2 rabbit squamous carcinoma model showed that paclitaxel incorporated into the outer lipid membrane of PFC nanoparticles was not effective for antiangiogenesis. Subsequent pharmacokinetic studies revealed the lack of efficacy to be related to significant drug loss in circulation with the premature release of the taxane occurring quicker and to a greater extent than for the more hydrophobic fumagillin.

Docetaxel (Dxtl) has a low solubility in water (<0.1 μg/mL) and from the synthetic stand point, chemistries involving esterification of the 2′-hydroxyl group, which is the most reactive of the all the available hydroxyl groups, are feasible. Conventional methods of protecting a hydroxyl group, such as esterification, can be utilized to protect this 2′-hydroxyl group, while leaving the hydroxyl groups at the positions 7 and 10 free for reaction. For the synthesis of docetaxel prodrug (Dxtl-PD), carbodiimide/4-dimethylaminopyridine (EDCI/DMAP) was the most efficient coupling efficient approach and produced the desired compound in 78% yield. The compound was isolated and purified by preparative thin layer chromatography (prep-TLC) and the structure was confirmed by NMR and ESI MS spectroscopy.[74]

The retention of the Dxtl-PD in the PFC nanoparticle during *in vitro* dissolution over 3 days in PBS with albumin or human plasma was excellent with <6% of prodrug released, indicating drug membrane stability.[74] These results are in contradistinction to the rapid release (~10%/day) of native paclitaxel from PFC nanoparticles under similar dissolution conditions.[26] Excess phospholipase A2 added to the incubation medium with Dxtl-PD nanoparticles produced negligible release of the drug. Furthermore, incubation of the Dxtl-PD nanoparticles in whole blood under slow continuous agitation imparted no passive prodrug transfer to erythrocytes through transient contact. When free Dxtl-PD was added to lipase rich plasma, docetaxel was liberated and differentiated from the parent prodrug. Regioselective

hydrolysis of the nanoparticle incorporating Dxtl-PD by PLA2 *in vitro* required the addition of 2-propranol to 'crack' the particle surfactant and expose the membrane components to the enzyme. Multiple peaks were observed showing that the Dxtl was hydrolyzed from the prodrug backbone including baccatin III (*m/z* 524 [M + Na]), which is a known degradation product in rats and humans.[75,76] These results support the model that Dxtl-PD is snuggled into the hydrophobic membrane protected from hydrolysis and lipase activation in blood until the nanoparticle is destabilized, such as with alcohol or by targeted binding.

The bioequivalence of paclitaxel, paclitaxel prodrug, docetaxel, or docetaxel prodrug at 0.5, 1, 5, 10, 50, and 100 μg/mL was studied in angiotensin II stimulated mouse vascular endothelial cells (2F2B) following 1 h of exposure with mild agitation.[74] No differences in endothelial proliferation were noted at 24, 48, and 72 h after exposure. The cytotoxicity of Dxtl-PD incorporated into PFC NPs was compared to Taxol® *in vitro* using 2F2B endothelial cell cultures stimulated with angiotensin II to upregulate activated $\alpha_v\beta_3$-integrin expression. $\alpha_v\beta_3$-Dxtl-PD NPs decreased ($P < 0.05$) cell proliferation 34% at 96 h compared with the saline control. The $\alpha_v\beta_3$-no-drug NPs had no effect on cell proliferation. At the equivalent low dose of taxane, Taxol® decreased cell proliferation less, 8%, which was similar to the controls but not significantly less than the $\alpha_v\beta_3$-Dxtl-PD NP (Figure 9).

In a followup experiment using angiotensin II-stimulated HUVEC cells, cell metabolic activity responses to docetaxel and Dxtl-PD NP were assessed at earlier time points: 48, 72, and 96 h. In that experiment, native docetaxel in methanol added to the medium was compared with its integrin-targeted lipase-labile prodrug analog on an equimolar drug basis. $\alpha_v\beta_3$-Dxtl-PD NPs, free docetaxel, and $\alpha_v\beta_3$-no drug NPs. $\alpha_v\beta_3$-Dxtl-PD NPs and free docetaxel equivalently decreased ($P < 0.05$) cell metabolic activity at 48 h compared with $\alpha_v\beta_3$-no drug NP. The marked reductions in cell metabolic activity persisted for both drug forms at 72 and 96 h. These results further substantiate the comparable bioequivalence of the native docetaxel and targeted Sn2 lipase-labile prodrug and suggest that the intracellular enzymatic hydrolysis requirement to achieve efficacy with Dxtl-PD was not limiting in the activated HUVEC cells.

The efficacy of the docetaxel Sn2 prodrug incorporated into the lipid membrane of $\alpha_v\beta_3$-targeted PFC nanoparticles ($\alpha_v\beta_3$-Dxtl-PD NP) was compared in the Vx2 rabbit tumor model to nontargeted Dxtl-PD NPs (NT-Dxtl-PD NP) and $\alpha_v\beta_3$-No Drug NPs. Animals were serially treated on days 9, 12, and 15 days post implant. On day 17, rabbits were imaged in

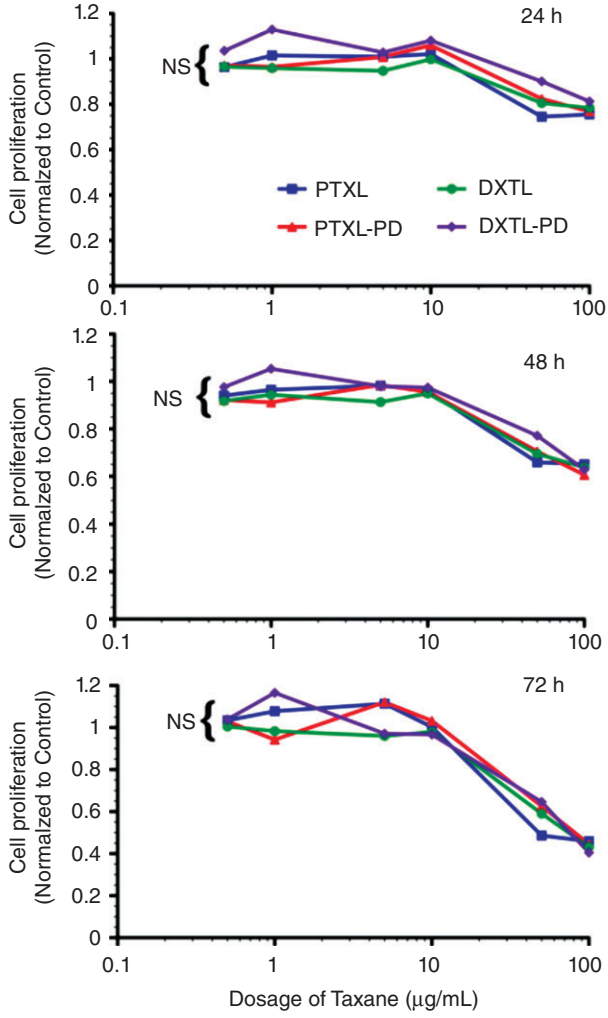

FIGURE 9 | Mouse vascular endothelial cells (2F2B) stimulated with angiotensin II (1nM) were treated with paclitaxel, docetaxel, paclitaxel prodrug, or docetaxel prodrug at 0.5, 1, 5, 10, 50, and 100 μg/mL for 1 h. Cultures were monitored for proliferation at 24, 48, and 72 h. No difference (P = NS) in biopotency of the different taxanes forms was detected. (Reprinted with permission from Ref 74. Copyright 2014)

a clinical 3 T MR scanner (Philips Achieva) using a high-resolution, T1-weighted, fat suppressed, 3D gradient echo sequence at baseline and 3 h after i.v. administration of $\alpha_v\beta_3$-Gd-DOTA nanoparticles (1 mL/kg), previously characterized and demonstrated *in vivo* (Figure 10).[77,78]

Angiogenesis contrast in the control animals was concentrated in the tumor periphery with minimal signal enhancement localized to the core, except for the rare lobulated tumor with an internal segment of neovascular-rich capsule. $\alpha_v\beta_3$-Dxtl-PD NPs substantially decreased ($P < 0.05$) MR detectable angiogenesis in the Vx2 tumor model after serial treatment, as opposed to the negative results achieved previously with the targeted particles incorporating

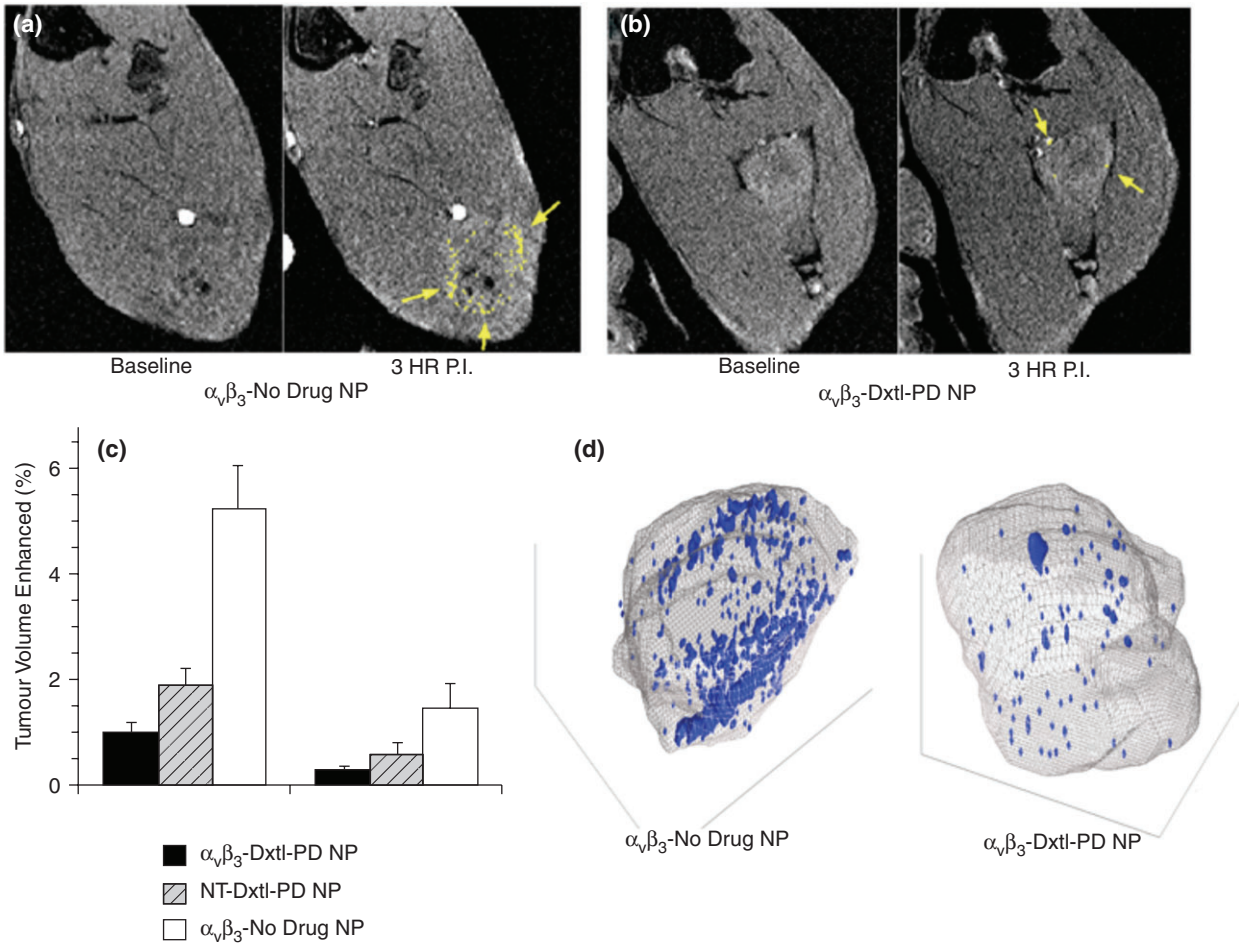

FIGURE 10 | (a) T1w MR images of Vx 2 tumor obtained at baseline and 3 hours after $\alpha_v\beta_3$-Gd-DOTA NP in animals receiving $\alpha_v\beta_3$-no drug NP showing peripheral tumor angiogenesis contrast enhancement false colored in yellow. (b) The same image sequence as panel (a) in Vx2 tumor rabbits following $\alpha_v\beta_3$-Dxtl-PD NP. (c) Histogram illustrating marked angiogenesis in the control rabbits rim (tumor peripheral 50%) versus those receiving Dtxl-PD with or without targeting. Note minimal contrast signal with the tumor core. Marked decrease in contrast in nontargeted (NT) animal group suggests that the dosage or frequency of treatment was in excess of the therapeutic need with passive entrapment providing adequate particle-to-endothelium contact to afford significant antiangiogenesis. (d) Representative three-dimensional neovascular maps of Vx2 tumor in control and targeted Dxtl-PD treatment groups. Note asymmetric distribution of confluent neovascular regions in the control rabbit note appreciated in the treated animal. Blue voxels equate to $\alpha_v\beta_3$-Gd-DOTA NP contrast enhancement exceeding three standard deviations over baseline. $^{*}P < 0.05$, $^{**}P < 0.01$. (Reprinted with permission from Ref 74. Copyright 2014)

native paclitaxel. NT-Dxtl-PD NP elicited neovascular suppression similar to $\alpha_v\beta_3$-Dxtl-PD NP, suggesting that the passive entrapment of the frequently dosed NT-Dxtl-PD NP provided enough sustained particle-endothelial cell contact under this serial regimen to afford prodrug transfer too low to be differentiated with MR molecular imaging at 3T. To verify that the antineovascular effect of the Dxtl-PD NPs observed MR molecular imaging was not attributable to the systemic premature release of taxane, a separate cohort of rabbits were implanted with the Vx2 tumor and treated serially with Abraxane® at an equimolar dose and compared to an independent saline control. MR molecular imaging of angiogenesis in this cohort on day 17 revealed no antiangiogenic effect with Abraxane®. Over this short study, no difference in tumor volume between any treatment groups was measured.[74]

Histological assessments of tumor showed that $\alpha_v\beta_3$-Dxtl-PD NP decreased ($P < 0.05$) tumor cell proliferation, as assessed by PNCA staining of the lesion, with the same trend noted for tumor apoptosis. The higher-sensitivity higher-resolution microscopic data indicated that targeted delivery of Dxtl-PD was biologically more effective than NT Dxtl-PD treatment, highlighting both the relative insensitivity of MR molecular imaging and the high potency of Dxtl-PD NPs (Figure 11).

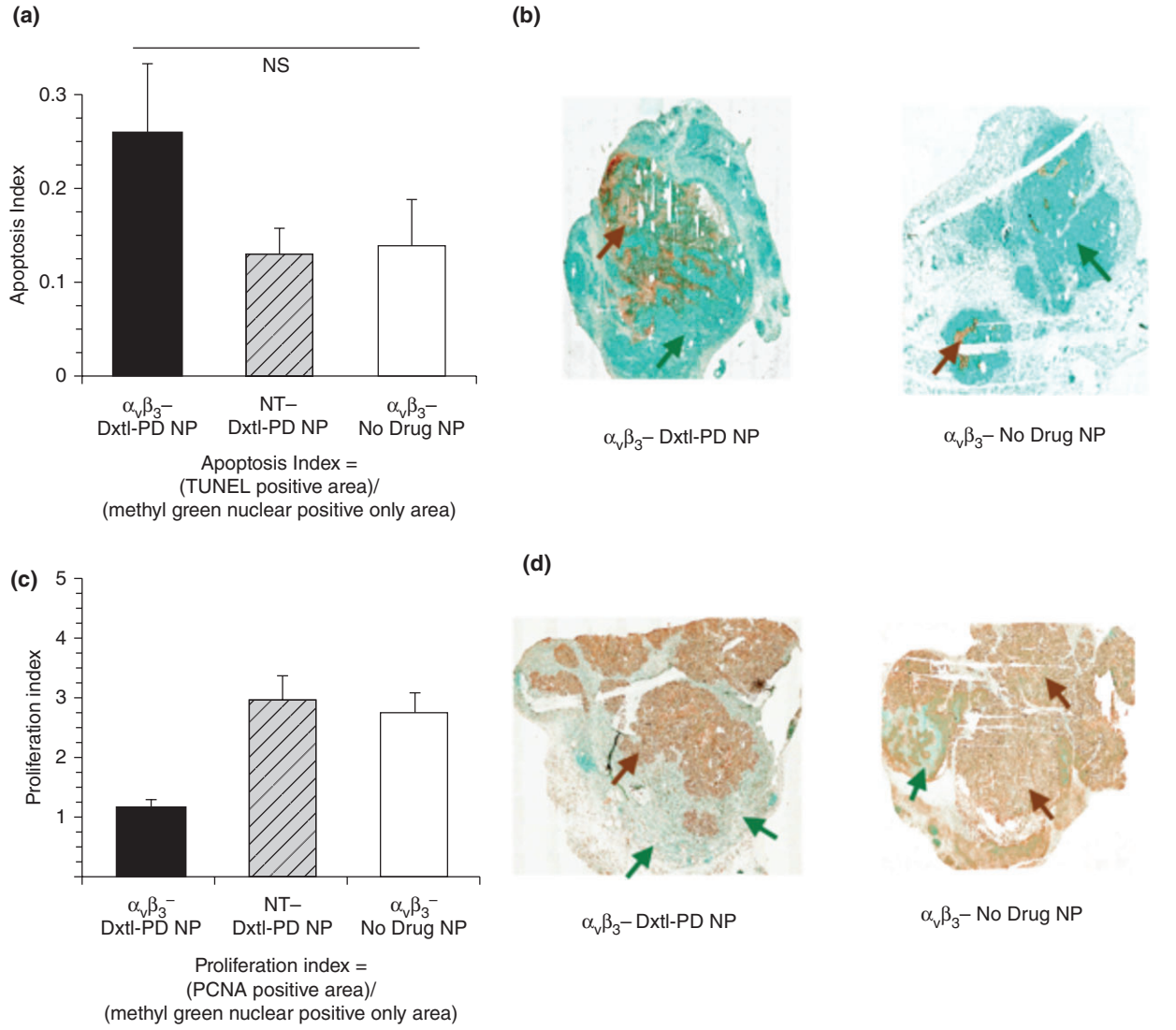

FIGURE 11 | (a) Histogram showing a trend (nonsignificant [NS], $P = 0.2$) toward increased apoptosis among Vx2 tumor rabbits receiving $\alpha_v\beta_3$-Dxtl-PD NP versus controls. (b) Illustrative sections (40×) of Vx2 tumor following TUNEL staining (brown arrows) using a methyl green nuclear positive reference for tumor area (green arrows). (c) Histogram showing a significant ($P < 0.05$) decrease in proliferation index among Vx2 tumor rabbits receiving $\alpha_v\beta_3$-Dxtl-PD NP versus controls. (d) Representative sections (40×) of Vx2 tumor following PCNA staining (brown arrows) using a methyl green nuclear positive reference for tumor area (green arrows). $^*P < 0.05$. (Reprinted with permission from Rf 74. Copyright 2014)

cMyc–Max Transcription Factor Antagonism in Myeloma

Multiple myeloma (MM) is a malignancy derived from a clone of plasma cells, which are terminally differentiated B-lymphocytes responsible for antibody production. As the second most common hematologic malignancy in the United States, MM accounts for 1% of cancer deaths. While recent therapeutic advances suggest future improvement, the current 5-year survival rate in patients with MM is less than 40%.[79] MM is initially responsive to several classes of chemotherapy, (e.g., proteasome inhibitors, immunomodulatory drugs [IMiDs], and alkylating agents), but eventually virtually all patients relapse and die from progressive disease.

The b-HLHZIP transcription factor c-Myc (*MYC*) is a powerful oncogene activated in many types of cancer, and is a central driver of myeloma development.[80] The expression of *MYC* increases with disease stage in MM, and *MYC* up-regulation likely plays an important role in the evolution of MGUS into MM.[81] *MYC* activation is likely to be an early event in myeloma pathogenesis with *MYC* rearrangement present in about 15% of newly diagnosed myeloma,[79,82] which may be an underestimation of the prevalence of *MYC* translocations.[83] The role of

MYC in MM was further indicated in a transgenic mouse model of myeloma with targeted activation of *MYC* in germinal center B-cells.[84]

In general, transcription factor's relative position downstream as integrators of multiple signaling cascades makes them an attractive therapeutic target which has been approached through antisense strategies,[85] RNA interference,[86] and interference with MYC–MAX dimerization using small molecules.[87] Transformation by MYC is dependent upon dimerization with the bHLHZIP protein MAX. MYC–MAX heterodimers bind to E-Boxes in the vicinity of target genes[88] to regulate their expression and to modulate numerous biological functions.[89–91]

The difficulty of inhibiting protein–protein or protein–DNA interactions with small molecules has made MYC a challenging therapeutic target.[92–95] Several small-molecule inhibitors of the MYC–MAX interaction were developed.[87,96–99] However, the development of these compounds experienced barriers of rapid systemic metabolism, significant toxicity, poor cancer bioavailability and an inability of the drug to reach intratumoral inhibitory concentrations.[99]

Given the potency of some MYC–MAX dimerization antagonists in cell-free assay, a Sn2 phospholipid prodrug nanomedicine strategy was considered to protect the compound in circulation and deliver it effectively into the target MM cells. An index compound (10058-F4) was synthesized and modified into the Sn2 prodrug form[100,101] Myc-inhibitor-1 prodrug (MI1-PD)(Figure 12).[37] The cytotoxic activities of the base compound, MI1, and the prodrug MI1-PD were evaluated and compared in human (H929 and U266) and mouse (5TGM1) MM cell lines at concentrations ranging from 1.0 nM to 100 μM. MTT cell viability assay showed that MI1-PD in DMSO decreased cell viability substantially more ($P < 0.05$) than MI1 in DMSO on an equimolar basis. Furthermore, MI1-PD induced significant apoptosis in the three MM cell lines, 92, 91, and 91% of control, respectively, whereas apoptosis was induced with MI1 was significantly less, 19, 31, and 31%, respectively ($P < 0.05$).[101]

As with all targeted therapies, nanotherapeutic delivery of MI1-PD is dependent upon the specific binding of nanoparticle to target cells. In this regard, the suitability $\alpha_v\beta_3$-integrin and $\alpha_4\beta_1$-integrin (VLA-4) target biomarkers was evaluated in aggressive human and mouse MM cells. Both integrins showed potential utility as targets for human MM in culture, but only $\alpha_4\beta_1$-integrin was adequately prevalent in the mouse 5TGM1 line, which was used below for *in vivo* study. The 5TGM1 MM is one of a series of transplantable murine myelomas arising spontaneously in C57BL/KaLwRij mice.[102–104] The therapeutic potential of VLA-4-targeted MI1-PD-containing NP was evaluated in KaLwRij mice inoculated intravenously with 5TGM1 cells and distributed into six groups. Mice were treated intravenously (50 μL of 20% suspension v/v) with targeted (T) or nontargeted (NT) PFC (200 nm) or micellar (20 nm) lipid-encapsulated particles that incorporated MI1-PD (D) or no drug (ND) on days 3, 5, 7,10,12, and 14. The following treatment cohorts were studied 1) ND/NT 200nm PFC NP; 2) T/ND 200nm PFC NP; 3) T/D 200nm PFC NP; 4) NT/ND 20nm micelles; 5) T/ND 20nm micelles, and 6) T/D 20nm micelles (Figure 13).[101] Disease progression was monitored by survival and serial measurements of serum paraprotein on day 17. Intravenously administered free MI1 and free MI1-PD offered no survival benefit for 5TGM1/KaLwRij myeloma mice versus the DMSO control. The tumor burden as reflected by serum immunoglobulin was decreased ($P < 0.05$) in mice treated with targeted MI1-PD NP as compared to nontargeted no drug NPs regardless of particle size, however, the best results were obtained with VLA-4-targeted MI1-PD micelles: (T/D 20: 52 days vs 29 days, $P = 0.001$) (Figure 14).

These results demonstrated a nanomedicine therapeutic approach to MM and for the first time showed reduced tumor burden in live mice using a potent MYC–MAX inhibitor. The Sn2 phospholipid prodrug MI1-PD significantly increased drug potency against myeloma cells in culture compared with its free drug counterpart, most likely due to increased cell bioavailability. When incorporated into lipid surfactant-coated nanoparticles and targeted to integrins, MI1-PD was most effective against cell lines strongly expressing the targeted biomarker, and less potent when receptor expression was low or absent. In an orthotopic mouse model of disseminated myeloma, administration of VLA-4-targeted MI1-PD NP conferred significant survival benefit versus nontargeted and drug-free controls, while neither MI1 nor MI1-PD provided any survival benefit when administered systemically as free compounds. These data provide a foundation to reconsider MYC transcription factor antagonism as a viable therapeutic strategy in MM and more broadly exemplify the potential of Nanomedicine approaches utilizing Sn-2 lipase labile prodrugs to overcome the poor solubility, poor systemic stability, poor biodistribution, or poor bioavailability that plague many therapeutic compounds.

CONCLUSION

Sn2 lipase labile phospholipid prodrugs in conjunction with CFDD offer an important advancement

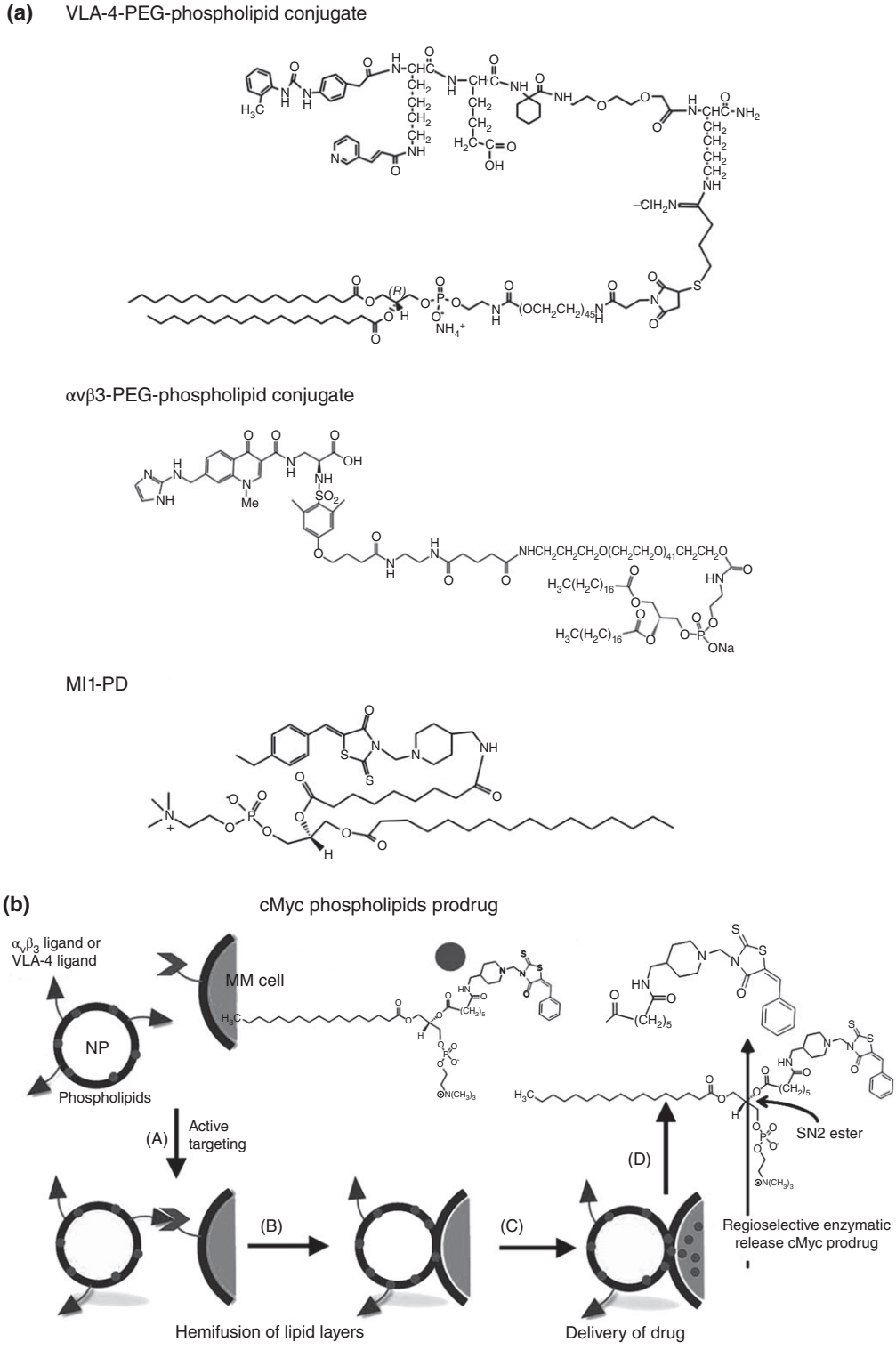

FIGURE 12 | (a) Chemical structures of VLA-4-PEG-phospholipid conjugate, $\alpha_v\beta_3$-PEG-phospholipid conjugate and MI1-PD. (b) Schematic representation illustrating nanoparticle (NP) design and lipid monolayer-mediated intracellular release of MYC-inhibitor from MI1-PD. The Myc prodrug (MI1-PD) from Panel a is represented by circles. The integrin-targeting ligands (VLA-4-PEG-phospholipid conjugate and $\alpha_v\beta_3$-PEG-phospholipid conjugate) from Panel a is represented by triangles. (A) Anti-Myc NPs are targeted by the homing ligand to myeloma (MM) cells expressing integrin proteins on their cell surface (represented by V). (B) Proximity induces hemifusion of lipid layers between NP and MM cells. (C) The MI1-PD in the NP membrane is then exposed to cellular lipases that (D) cleave the phospholipid moiety of the prodrug and release the anti-Myc moiety into the MM cell.[100]

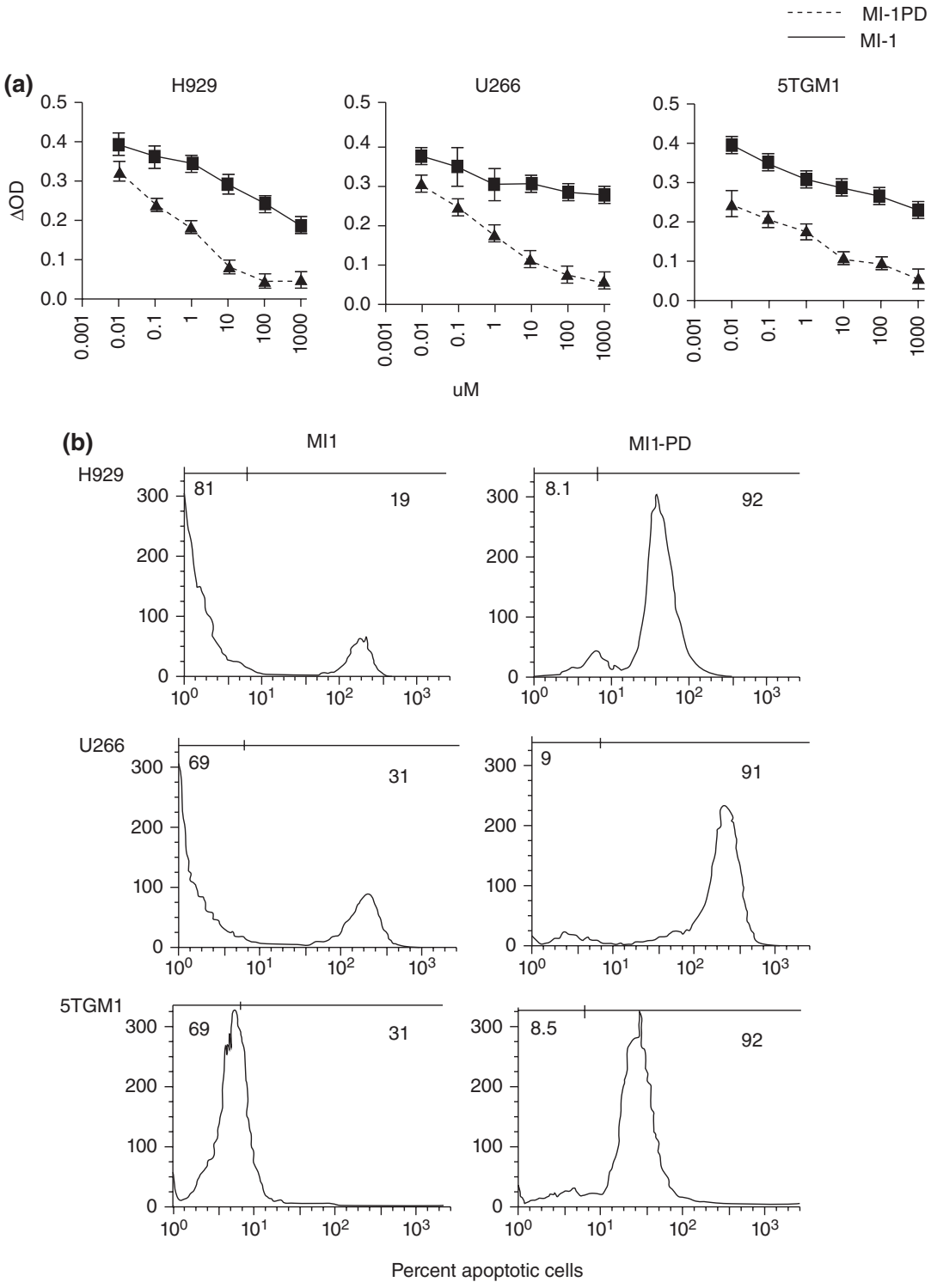

FIGURE 13 | Myc inhibitor 1 (MI1) and MI1 prodrug (MI1-PD) decrease viability and induce apoptosis in myeloma cell lines. (a) MTT assay for cell viability at 24 h with MI1 and MI1-PD at given concentrations in H929, U266, and 5TGM1 cells. Values are average of three separate experiments in triplicates and expressed as mean ± SD. $^{*}P < 0.05$. (b) Representative of Annexin V-PE staining of cells for apoptosis following MI1 and MI1-PD treatment (left and right columns respectively) at given concentrations in H929, U266, and 5TGM1 cells at 24 h. (Reprinted with permission from Ref 101. Copyright 2014)

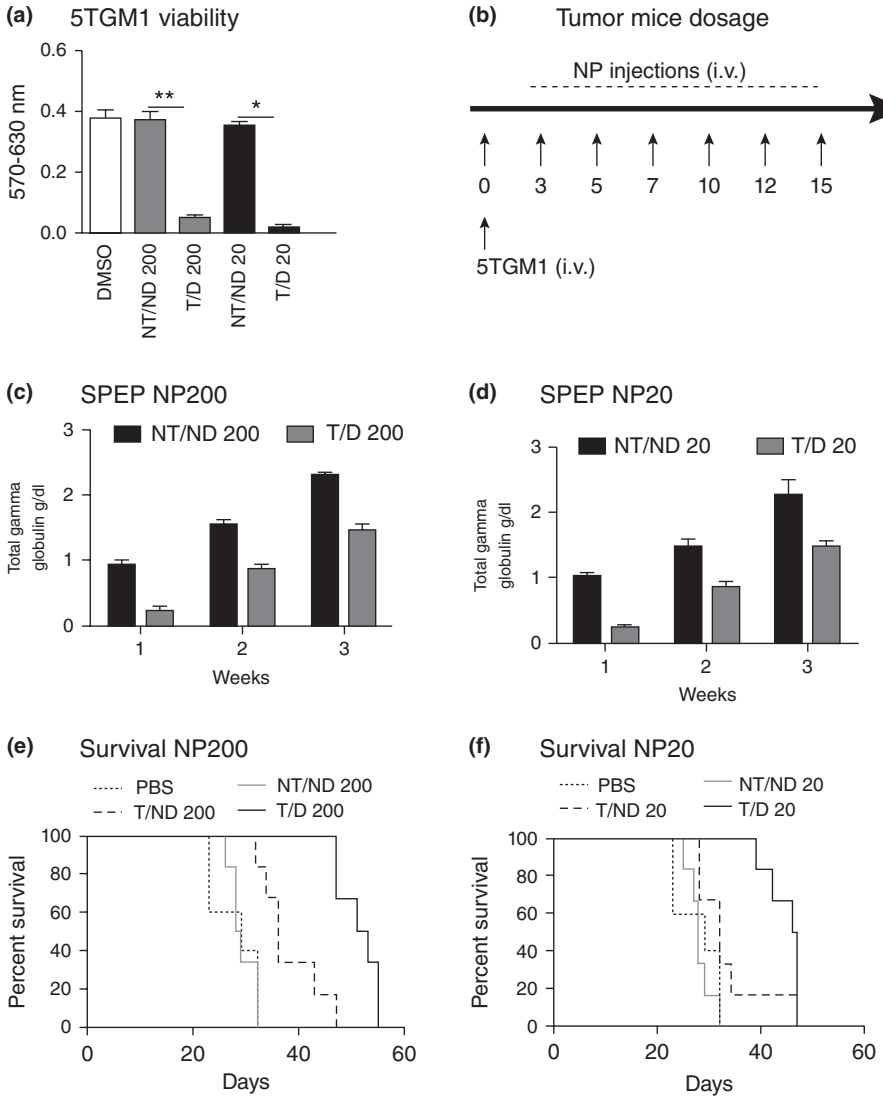

FIGURE 14 | Anti-MYC NPs prolong survival in a mouse model of multiple myeloma. (a) MTT studies in 5TGM1 cells at 24 h. (b) The experimental protocol for the *in vivo* tumor growth assay. The groups were as follows: (1) ND/NT 200; (2) T/ND 200; (3) T/D 200; (4) NT/ND 20; (5) T/ND 20; and (6) T/D 20 all injected on days 3, 5, 7, 10, 12, and 14 following the i.v. injections of 5TGM1 cells (day 0) (c, d) SPEP quantification of each treatment groups 3 days after the last injection was given (each dot represents SPEP value for one mouse). (e, f) Kaplan–Meier survival curves of the treated mice with 20 and 200 nm NPs. (Reprinted with permission from Ref 101. Copyright 2014)

in Nanomedicine. Often drugs incorporated into nanosystems, targeted or not, are lost during circulation to the target and these systems have morphed into prolonged release nanoexcipients that favorably alter the pharmacokinetics and volume of distribution of drugs yielding greater efficacy and lower toxicity. Sn2 phospholipid prodrugs favorably address premature drug loss and inadequate target cell bioavailability for lipid-encapsulated nanoemulsions for both nanomedicines constrained by design to vascular accessible targets like the neovasculature, as well as for particles essentially the size of proteins which, penetrate through naturally fenestrated endothelium, as found in the bone marrow or inflamed thin-walled venules of the microcirculation to reach extravascular targets.

Twenty years ago, the concept of specifically targeting a particle to any biological marker was considered a hope. Today, innumerable nanomedicines accomplish this feat in preclinical animal models. The prospects for Nanomedicine therapies to address intractable medical issues, such a MM, have never been better. Nanomedicine has finally made 'made the turn' toward meaningful success.

REFERENCES

1. Gabizon A, Catane R, Uziely B, Kaufman B, Safra T, Cohen R, Martin F, Huang A, Barenholz Y. Prolonged circulation time and enhanced accumulation in malignant exudates of doxorubicin encapsulated in polyethylene-glycol coated liposomes. *Cancer Res* 1994, 54:987–992.
2. Ibrahim NK, Desai N, Legha S, Soon-Shiong P, Theriault RL, Rivera E, Esmaeli B, Ring SE, Bedikian A, Hortobagyi GN, et al. Phase I and pharmacokinetic study of ABI-007, a cremophor-free, protein-stabilized, nanoparticle formulation of paclitaxel. *Clin Cancer Res* 2002, 8:1038–1044.
3. Suzuki S, Watanabe S, Uno S, Tanaka M, Masuko T, Hashimoto Y. Endocytosis does not necessarily augment the cytotoxicity of adriamycin encapsulated in immunoliposomes. *Biochim Biophys Acta* 1994, 1224:445–453.
4. Abes R, Arzumanov AA, Moulton HM, Abes S, Ivanova GD, Iversen PL, Gait MJ, Lebleu B. Cell-penetrating-peptide-based delivery of oligonucleotides: an overview. *Biochem Soc Trans* 2007, 35: 775–779.
5. Wiethoff CM, Middaugh CR. Barriers to nonviral gene delivery. *J Pharm Sci* 2003, 92:203–217.
6. El-Sayed A, Khalil IA, Kogure K, Futaki S, Harashima H. Octaarginine- and octalysine-modified nanoparticles have different modes of endosomal escape. *J Biol Chem* 2008, 283:23450–23461.
7. Hatakeyama H, Ito E, Akita H, Oishi M, Nagasaki Y, Futaki S, Harashima H. A pH-sensitive fusogenic peptide facilitates endosomal escape and greatly enhances the gene silencing of siRNA-containing nanoparticles in vitro and in vivo. *J Control Release* 2009, 139:127–132.
8. Kobayashi S, Nakase I, Kawabata N, Yu HH, Pujals S, Imanishi M, Giralt E, Futaki S. Cytosolic targeting of macromolecules using a pH-dependent fusogenic peptide in combination with cationic liposomes. *Bioconjug Chem* 2009, 20:953–959.
9. Rosenholm JM, Peuhu E, Eriksson JE, Sahlgren C, Lindén M. Targeted intracellular delivery of hydrophobic agents using mesoporous hybrid silica nanoparticles as carrier systems. *Nano Lett* 2009, 9:3308–3311.
10. Wang XL, Xu R, Lu ZR. A peptide-targeted delivery system with pH-sensitive amphiphilic cell membrane disruption for efficient receptor-mediated siRNA delivery. *J Control Release* 2009, 134:207–213.
11. Adler AF, Leong KW. Emerging links between surface nanotechnology and endocytosis: impact on nonviral gene delivery. *Nano Today* 2010, 5:553–569.
12. Dehousse V, Garbacki N, Colige A, Evrard B. Development of pH-responsive nanocarriers using trimethylchitosans and methacrylic acid copolymer for siRNA delivery. *Biomaterials* 2010, 31:1839–1849.
13. Shim MS, Kwon YJ. Acid-transforming polypeptide micelles for targeted nonviral gene delivery. *Biomaterials* 2010, 31:3404–3413.
14. Krpetić Z, Saleemi S, Prior IA, Sée V, Qureshi R, Brust M. Negotiation of intracellular membrane barriers by TAT-modified gold nanoparticles. *ACS Nano* 2011, 5:5195–5201.
15. Lehto T, Simonson OE, Mäger I, Ezzat K, Sork H, Copolovici DM, Viola JR, Zaghloul EM, Lundin P, Moreno PMD, et al. A peptide-based vector for efficient gene transfer in vitro and in vivo. *Mol Ther* 2011, 19:1457–1467.
16. Liu J, Jiang Z, Zhou J, Zhang S, Saltzman WM. Enzyme-synthesized poly(amine-co-esters) as nonviral vectors for gene delivery. *J Biomed Mater Res A* 2011, 96(A):456–465.
17. Bakhru SH, Altiok E, Highley C, Delubac D, Suhan J, Kevin Hitchens T, Ho C, Zappe S. Enhanced cellular uptake and long-term retention of chitosan-modified iron-oxide nanoparticles for MRI-based cell tracking. *Int J Nanomed* 2012, 7:4613–4623.
18. Curcio A, Marotta R, Riedinger A, Palumberi D, Falqui A, Pellegrino T. Magnetic pH-responsive nanogels as multifunctional delivery tools for small interfering RNA (siRNA) molecules and iron oxide nanoparticles (IONPs). *Chem Commun* 2012, 48: 2400–2402.
19. Li Y, Wang J, Wientjes MG, Au JLS. Delivery of nanomedicines to extracellular and intracellular compartments of a solid tumor. *Adv Drug Deliv Rev* 2012, 64:29–39.
20. Luo Z, Cai K, Hu Y, Li J, Ding X, Zhang B, Xu D, Yang W, Liu P. Redox-responsive molecular nanoreservoirs for controlled intracellular anticancer drug delivery based on magnetic nanoparticles. *Adv Mater* 2012, 24:431–435.
21. Shrestha R, Elsabahy M, Florez-Malaver S, Samarajeewa S, Wooley KL. Endosomal escape and siRNA delivery with cationic shell crosslinked knedel-like nanoparticles with tunable buffering capacities. *Biomaterials* 2012, 33:8557–8568.
22. Gilleron J, Querbes W, Zeigerer A, Borodovsky A, Marsico G, Schubert U, Manygoats K, Seifert S, Andree C, Stöter M, et al. Image-based analysis of lipid nanoparticle-mediated siRNA delivery, intracellular trafficking and endosomal escape. *Nat Biotechnol* 2013, 31:638–646.
23. Peetla C, Jin S, Weimer J, Elegbede A, Labhasetwar V. Biomechanics and thermodynamics of nanoparticle interactions with plasma and endosomal membrane lipids in cellular uptake and endosomal escape. *Langmuir* 2014, 30:7522–7532.
24. Ahmad A, Ranjan S, Zhang W, Zou J, Pyykkö I, Kinnunen PKJ. Novel endosomolytic peptides for

enhancing gene delivery in nanoparticles. *Biochim Biophys Acta* 2015, 1848:544–553.

25. Ortega RA, Barham WJ, Kumar B, Tikhomirov O, McFadden ID, Yull FE, Giorgio TD. Biocompatible mannosylated endosomal-escape nanoparticles enhance selective delivery of short nucleotide sequences to tumor associated macrophages. *Nanoscale* 2015, 7:500–510.
26. Lanza GM, Yu X, Winter PM, Abendschein DR, Karukstis KK, Scott MJ, Chinen LK, Fuhrhop RW, Scherrer DE, Wickline SA. Targeted antiproliferative drug delivery to vascular smooth muscle cells with a magnetic resonance imaging nanoparticle contrast agent: implications for rational therapy of restenosis. *Circulation* 2002, 106:2842–2847.
27. Partlow K, Lanza G, Wickline S. Exploiting lipid raft transport with membrane targeted nanoparticles: a strategy for cytosolic drug delivery. *Biomaterials* 2008, 29:3367–3375.
28. Soman N, Marsh J, Lanza G, Wickline S. New mechanisms for nonporative ultrasound stimulation of cargo delivery to cell cytosol with targeted perfluorocarbon nanoparticles. *Nanotechnology* 2008, 19: 185102–185107.
29. Winter PM, Schmieder AH, Caruthers SD, Keene JL, Zhang H, Wickline SA, Lanza GM. Minute dosages of alpha(nu) beta 3-targeted fumagillin nanoparticles impair Vx-2 tumor angiogenesis and development in rabbits. *FASEB J* 2008, 22:2758–2767.
30. Winter P, Neubauer A, Caruthers S, Harris T, Robertson J, Williams T, Schmieder A, Hu G, Allen J, Lacy E, et al. Endothelial alpha(nu) beta (3)-integrin targeted fumagillin nanoparticles inhibit angiogenesis in atherosclerosis. *Arterioscler Thromb Vasc Biol* 2006, 26:2103–2109.
31. Zhou HF, Chan HW, Wickline SA, Lanza GM, Pham CT. Alpha v beta 3-targeted nanotherapy suppresses inflammatory arthritis in mice. *FASEB J* 2009, 23:2978–2985.
32. Bhargava P, Marshall JL, Rizvi N, Dahut W, Yoe J, Figuera M, Phipps K, Ong VS, Kato A, Hawkins MJ. A Phase I and pharmacokinetic study of TNP-470 administered weekly to patients with advanced cancer. *Clin Cancer Res* 1999, 5:1989–1995.
33. Kudelka AP, Verschraegen CF, Loyer E. Complete remission of metastatic cervical cancer with the angiogenesis inhibitor TNP-470. *N Engl J Med* 1998, 338:991–992.
34. Offodile R, Walton T, Lee M, Stiles A, Nguyen M. Regression of metastatic breast cancer in a patient treated with the anti-angiogenic drug TNP-470. *Tumori* 1999, 85:51–53.
35. Pan D, Sanyal N, Schmieder AH, Senpan A, Kim B, Yang X, Hu G, Allen JS, Gross RW, Wickline SA, et al. Antiangiogenic nanotherapy with lipase-labile Sn-2 fumagillin prodrug. *Nanomedicine* 2012, 7:1507–1519.
36. Burke J, Dennis E. Phospholipase A_2 biochemistry. *Cardiovasc Drugs Ther* 2009, 23:49–59.
37. Wymer NJ, Gerasimov OV, Thompson DH. Cascade liposomal triggering: Light-induced Ca^{2+} release from diplasmenylcholine liposomes triggers PLA_2-catalyzed hydrolysis and contents leakage from DPPC liposomes. *Bioconjug Chem* 1998, 9:305–308.
38. Davidsen J, Jørgensen K, Andresen TL, Mouritsen OG. Secreted phospholipase A_2 as a new enzymatic trigger mechanism for localised liposomal drug release and absorption in diseased tissue. *Biochim Biophys Acta* 2003, 1609:95–101.
39. Andresen TL, Davidsen J, Begtrup M, Mouritsen OG, Jørgensen K. Enzymatic release of antitumor ether lipids by specific phospholipase A_2 activation of liposome-forming prodrugs. *J Med Chem* 2004, 47: 1694–1703.
40. Jensen SS, Andresen TL, Davidsen J, Høyrup P, Shnyder SD, Bibby MC, Gill JH, Jørgensen K. Secretory phospholipase A_2 as tumor-specific trigger for targeted delivery of a novel class of liposomal prodrug anticancer ether lipids. *Mol Cancer Ther* 2004, 3: 1451–1458.
41. Andresen TL, Jørgensen K. Synthesis and membrane behavior of a new class of unnatural phospholipid analogs useful as phospholipase A_2 degradable liposomal drug carriers. *BBA - Biomembranes* 2005, 1669:1–7.
42. Andresen TL, Jensen SS, Madsen R, Jorgensen K. Synthesis and biological activity of anticancer ether lipids that are specifically released by phospholipase A_2 in tumor tissue. *J Med Chem* 2005, 48:7305–7314.
43. Peters G, Møller M, Jørgensen K, Rönnholm P, Mikkelsen M, Andresen T. Secretory phospholipase A_2 hydrolysis of phospholipid analogues is dependent on water accessibility to the active site. *J Am Chem Soc* 2007, 129:5451–5461.
44. Kaasgaard T, Andresen TL, Jensen SS, Holte RO, Jensen LT, Jørgensen K. Liposomes containing alkylated methotrexate analogues for phospholipase A_2 mediated tumor targeted drug delivery. *Chem Phys Lipids* 2009, 157:94–103.
45. Linderoth L, Peters GH, Madsen R, Andresen TL. Drug delivery by an enzyme-mediated cyclization of a lipid prodrug with unique bilayer-formation properties. *Angew Chem Int Ed* 2009, 48:1823–1826.
46. Pedersen PJ, Christensen MS, Ruysschaert T, Linderoth L, Andresen TL, Melander F, Mouritsen OG, Madsen R, Clausen MH. Synthesis and biophysical characterization of chlorambucil anticancer ether lipid prodrugs. *J Med Chem* 2009, 52:3408–3415.
47. Pedersen PJ, Adolph SK, Subramanian AK, Arouri A, Andresen TL, Mouritsen OG, Madsen R, Madsen MW, Peters GH, Clausen MH. Liposomal formulation of retinoids designed for enzyme triggered release. *J Med Chem* 2010, 53:3782–3792.

48. Madsen JJ, Linderoth L, Subramanian AK, Andresen TL, Peters GH. Secretory phospholipase A_2 activity toward diverse substrates. *J Phys Chem B* 2011, 115:6853–6861.
49. Arik D, Duvdevani R, Shapiro I, Elmann A, Finkelstein E, Hoffman A. The oral absorption of phospholipid prodrugs: in vivo and in vitro mechanistic investigation of trafficking of a lecithin-valproic acid conjugate following oral administration. *J Control Release* 2008, 126:1–9.
50. Dahan A, Duvdevani R, Dvir E, Elmann A, Hoffman A. A novel mechanism for oral controlled release of drugs by continuous degradation of a phospholipid prodrug along the intestine: in-vivo and in-vitro evaluation of an indomethacin–lecithin conjugate. *J Control Release* 2007, 119:86–93.
51. Gabizon AA, Tzemach D, Horowitz AT, Shmeeda H, Yeh J, Zalipsky S. Reduced toxicity and superior therapeutic activity of a mitomycin c lipid-based prodrug incorporated in pegylated liposomes. *Clin Cancer Res* 2006, 12:1913–1920.
52. Zalipsky S, Saad M, Kiwan R, Ber E, Yu N, Minko T. Antitumor activity of new liposomal prodrug of mitomycin c in multidrug resistant solid tumor: insights of the mechanism of action. *J Drug Target* 2007, 15:518–530.
53. Gabizon A, Amitay Y, Tzemach D, Gorin J, Shmeeda H, Zalipsky S. Therapeutic efficacy of a lipid-based prodrug of mitomycin c in pegylated liposomes: studies with human gastro-entero-pancreatic ectopic tumor models. *J Control Release* 2012, 160:245–253.
54. Herbst RS, Madden TL, Tran HT, Blumenschein GR Jr, Meyers CA, Seabrooke LF, Khuri FR, Puduvalli VK, Allgood V, Fritsche HA Jr, et al. Safety and pharmacokinetic effects of TNP-470, an angiogenesis inhibitor, combined with paclitaxel in patients with solid tumors: evidence for activity in non-small-cell lung cancer. *J Clin Oncol* 2002, 20:4440–4447.
55. Logothetis CJ, Wu KK, Finn LD, Daliani D, Figg W, Ghaddar H, Gutterman JU. Phase I trial of the angiogenesis inhibitor TNP-470 for progressive androgen-independent prostate cancer. *Clin Cancer Res* 2001, 7:1198–1203.
56. Winter P, Caruthers S, Zhang H, Williams T, Wickline S, Lanza G. Antiangiogenic synergism of integrin-targeted fumagillin nanoparticles and atorvastatin in atherosclerosis. *J Am Coll Cardiol Img* 2008, 1:624–634.
57. Zhang R, Pan D, Cai X, Yang X, Senpan A, Allen JS, Lanza GM, Wang LV. Alpha nu beta 3-targeted copper nanoparticles incorporating an Sn 2 lipase-labile fumagillin prodrug for photoacoustic neovascular imaging and treatment. *Theranostics* 2015, 5: 124–133.
58. Pan D, Pramanik M, Senpan A, Allen JS, Zhang H, Wickline SA, Wang LV, Lanza GM. Molecular photoacoustic imaging of angiogenesis with integrin-targeted gold nanobeacons. *FASEB J* 2011, 25:875–882.
59. Jain RK. Taming vessels to treat cancer. *Sci Am* 2008, 298:56–63.
60. Jain RK, Finn AV, Kolodgie FD, Gold HK, Virmani R. Antiangiogenic therapy for normalization of atherosclerotic plaque vasculature: a potential strategy for plaque stabilization. *Nat Clin Pract Cardiovasc Med* 2007, 4:491–502.
61. Jain R. Normalizing tumor vasculature with anti-angiogenic therapy: a new paradigm for combination therapy. *Nat Med* 2001, 7:987–989.
62. Monach P, Hattori K, Huang H, Hyatt E, Morse J, Nguyen L, Ortiz-lpoez A, Wu H, Mathis D, Benoist C. The K/BXN mouse model of inflammatory arthritis: theory and practice. *Methods Mol Med* 2007, 136:269–282.
63. Zhou HF, Yan H, Senpan A, Wickline SA, Pan D, Lanza GM, Pham CT. Suppression of inflammation in a mouse model of rheumatoid arthritis using targeted lipase-labile fumagillin prodrug nanoparticles. *Biomaterials* 2012, 33:8632–8640.
64. Bernier SG, Lazarus DD, Clark E, Doyle B, Labenski MT, Thompson CD, Westlin WF, Hannig G. A methionine aminopeptidase-2 inhibitor, PPI-2458, for the treatment of rheumatoid arthritis. *Proc Natl Acad Sci USA* 2004, 101:10768–10773.
65. Bainbridge J, Madden L, Essex D, Binks M, Malhotra R, Paleolog EM. Methionine aminopeptidase-2 blockade reduces chronic collagen-induced arthritis: potential role for angiogenesis inhibition. *Arthritis Res Ther* 2007, 9:R127.
66. Zhou H, Yan H, Hu Y, Springer L, Yang X, Wickline S, Pan D, Lanza G, Pham C. Fumagillin prodrug nanotherapy suppresses macrophage inflammatory response via endothelial nitric oxide. *ACS Nano* 2014, 8:7305–7317.
67. Zhou HF, Hu G, Wickline SA, Lanza GM, Pham CT. Synergistic effect of antiangiogenic nanotherapy combined with methotrexate in the treatment of experimental inflammatory arthritis. *Nanomedicine (Lond)* 2010, 5:1065–1074.
68. Lee J, Ku T, Yu H, Chong K, Ryu SW, Choi K, Choi C. Blockade of VEGF-A suppresses tumor growth via inhibition of autocrine signaling through Fak and Akt. *Cancer Lett* 2012, 318:221–225.
69. Eskens FA, Verweij J. The clinical toxicity profile of vascular endothelial growth factor (VEGF) and vascular endothelial growth factor receptor (VEGFR) targeting angiogenesis inhibitors; a review. *Eur J Cancer* 2006, 42:3127–3139.
70. Jones SE, Erban J, Overmoyer B, Budd GT, Hutchins L, Lower E, Laufman L, Sundaram S, Urba WJ, Pritchard KI, et al. Randomized phase III study of docetaxel compared with paclitaxel in metastatic breast cancer. *J Clin Oncol* 2005, 23:5542–5551.

71. Stone GW, Ellis SG, Cox DA, Hermiller J, O'Shaughnessy C, Mann JT, Turco M, Caputo R, Bergin P, Greenberg J, et al. A polymer-based, paclitaxel-eluting stent in patients with coronary artery disease. *N Engl J Med* 2004, 350:221–231.
72. Lanza GM, Winter PM, Caruthers SD, Hughes MS, Hu G, Schmieder AH, Wickline SA. Theragnostics for tumor and plaque angiogenesis with perfluorocarbon nanoemulsions. *Angiogenesis* 2010, 13:189–202.
73. Lanza GM, Caruthers SD, Winter PM, Hughes MS, Schmieder AH, Hu G, Wickline SA. Angiogenesis imaging with vascular-constrained particles: the why and how. *Eur J Nucl Med Mol Imaging* 2010, 37(Suppl 1):S114–S126.
74. Pan D, Schmieder A, Wang K, Yang X, Senpan A, Cui G, Killgore K, Kim B, Allen J, Zhang H, et al. Anti-angiogenesis therapy in the Vx2 rabbit cancer model with a lipase-cleavable Sn 2 taxane phospholipid prodrug using $\alpha v\beta 3$-targeted theranostic nanoparticles. *Theranostics* 2014, 4:565–578.
75. Cresteil T, Monsarrat B, Dubois J, Sonnier M, Alvinerie P, Gueritte F. Regioselective metabolism of taxoids by human CYP3a4 and 2c8: structure–activity relationship. *Drug Metab Dispos* 2002, 30:438–445.
76. Hendrikx JJMA, Dubbelman A-C, Rosing H, Schinkel AH, Schellens JHM, Beijnen JH. Quantification of docetaxel and its metabolites in human plasma by liquid chromatography/tandem mass spectrometry. *Rapid Commun Mass Spectrom* 2013, 27:1–10.
77. Schmieder AH, Caruthers SD, Zhang H, Williams TA, Robertson JD, Wickline SA, Lanza GM. Three-dimensional mr mapping of angiogenesis with alpha 5 beta 1(alpha nu beta 3)-targeted theranostic nanoparticles in the MDA-MB-435 xenograft mouse model. *FASEB J* 2008, 22:4179–4189.
78. Schmieder AH, Winter PM, Williams TA, Allen JS, Hu G, Zhang H, Caruthers SD, Wickline SA, Lanza GM. Molecular MR imaging of neovascular progression in the Vx2 tumor with alpha v beta 3-targeted paramagnetic nanoparticles. *Radiology* 2013, 268:470–480.
79. Edwards B, Ward E, Kohler B, Eheman C, Zauber A, Anderson R, Jemal A, Schymura M, Lansdorp-Vogelaar I, Seeff L, van Ballegooijen M, Goede S, Ries L. Annual report to the nation on the status of cancer, 1975–2006, featuring colorectal cancer trends and impact of interventions (risk factors, screening, and treatment) to reduce future rates. *Cancer* 2010, 116:544–573.
80. Kuehl WM. Mouse models can predict cancer therapy. *Blood* 2012, 120:238–240.
81. Anguiano A, Tuchman SA, Acharya C, Salter K, Gasparetto C, Zhan F, Dhodapkar M, Nevins J, Barlogie B, Shaughnessy JD Jr, et al. Gene expression profiles of tumor biology provide a novel approach to prognosis and may guide the selection of therapeutic targets in multiple myeloma. *J Clin Oncol* 2009, 27: 4197–4203.
82. Chng WJ, Huang GF, Chung TH, Ng SB, Gonzalez-Paz N, Troska-Price T, Mulligan G, Chesi M, Bergsagel PL, Fonseca R. Clinical and biological implications of MYC activation: a common difference between MGUS and newly diagnosed multiple myeloma. *Leukemia* 2011, 25:1026–1035.
83. Dib A, Gabrea A, Glebov OK, Bergsagel PL, Kuehl WM. Characterization of MYC translocations in multiple myeloma cell lines. *J Natl Cancer Inst Monogr* 2008:25–31.
84. Avet-Loiseau H, Attal M, Moreau P, Charbonnel C, Garban F, Hulin C, Leyvraz S, Michallet M, Yakoub-Agha I, Garderet L, et al. Genetic abnormalities and survival in multiple myeloma: the experience of the intergroupe francophone du myelome. *Blood* 2007, 109:3489–3495.
85. Chen JP, Lin C, Xu CP, Zhang XY, Fu M, Deng YP, Wei Y, Wu M. Molecular therapy with recombinant antisense c-Myc adenovirus for human gastric carcinoma cells in vitro and in vivo. *J Gastroenterol Hepatol* 2001, 16:22–28.
86. Lewis DL, Hagstrom JE, Loomis AG, Wolff JA, Herweijer H. Efficient delivery of siRNA for inhibition of gene expression in postnatal mice. *Nat Genet* 2002, 32:107–108.
87. Berg T, Cohen SB, Desharnais J, Sonderegger C, Maslyar DJ, Goldberg J, Boger DL, Vogt PK. Small-molecule antagonists of MYC/MAX dimerization inhibit Myc-induced transformation of chicken embryo fibroblasts. *Proc Natl Acad Sci USA* 2002, 99: 3830–3835.
88. Murre C, McCaw PS, Baltimore D. A new DNA binding and dimerization motif in immunoglobulin enhancer binding, daughterless, MYOD, and MYC proteins. *Cell* 1989, 56:777–783.
89. Amati B, Littlewood TD, Evan GI, Land H. The c-Myc protein induces cell cycle progression and apoptosis through dimerization with Max. *EMBO J* 1993, 12:5083–5087.
90. Freytag SO, Dang CV, Lee WM. Definition of the activities and properties of c-Myc required to inhibit cell differentiation. *Cell Growth Differ* 1990, 1: 339–343.
91. Smith MJ, Charron-Prochownik DC, Prochownik EV. The leucine zipper of c-Myc is required for full inhibition of erythroleukemia differentiation. *Mol Cell Biol* 1990, 10:5333–5339.
92. Hermeking H. The MYC oncogene as a cancer drug target. *Curr Cancer Drug Targets* 2003, 3:163–175.
93. Prochownik EV. C-Myc as a therapeutics target in cancer. *Expert Rev Anticancer Ther* 2004, 4:289–302.
94. Darnell JE, Jr. Transcription factors as targets for cancer therapy. *Nat Rev Cancer* 2002, 2:740–749.
95. Gibbs JB. Mechanism-based target identification and drug discovery in cancer research. *Science* 2000, 287: 1969–1973.

96. Kiessling A, Sperl B, Hollis A, Eick D, Berg T. Selective inhibition of c-Myc/Max dimerization and DNA binding by small molecules. *Chem Biol* 2006, 13: 745–751.

97. Bagnasco L, Tortolina L, Biasotti B, Castagnino N, Ponassi R, Tomati V, Nieddu E, Stier G, Malacarne D, Parodi S. Inhibition of a protein-protein interaction between NI1 and c-MTC by small peptidomimetic molecules inspired by helix-1 of c-MYC: identification of a new target of potential antineoplastic interest. *FASEB J* 2007, 21:1256–1263.

98. Yin X, Giap C, Lazo JS, Prochownik EV. Low molecular weight inhibitors of MYC–MAX interaction and function. *Oncogene* 2003, 22:6151–6159.

99. Clausen DM, Guo J, Parise RA, Beumer JH, Egorin MJ, Lazo JS, Prochownik EV, Eiseman JL. In vitro cytotoxicity and in vivo efficacy, pharmacokinetics, and metabolism of 10074-G5, a novel small-molecule inhibitor of c-MYC/MAX dimerization. *J Pharmacol Exp Ther* 2010, 335:715–727.

100. Pan D, Kim B, Hu G, Sood-Gupta D, Senpan A, Schmieder A, Swain C, Wickline S, Tomasson M, Lanza G. A strategy for combating melanoma with oncogenic c-Myc inhibitors and targeted nanotherapy. *Nanomedicine (Lond)* 2015, 10:241–251.

101. Soodgupta D, Pan D, Cui G, Senpan A, Yang X, Lu L, Weilbaecher KN, Prochownik EV, Lanza GM, Tomasson MH. Small molecule MYC inhibitor conjugated to integrin-targeted nanoparticles extends survival in a mouse model of disseminated multiple myeloma. *Mol Cancer Ther* 2015, 14:1286–1294.

102. Radl J, de Glopper E, Schuit HER, Zurcher C. Idiopathic paraprotienemia, ii. transplantation of the paraprotein-producing clone from old to young C587BL/Kalwrij mice. *J Immunol* 1979, 122: 609–613.

103. Radl J, Croese JW, Zurcher C, Van Den Enden-Vieveen MHM, Margreet de Leeuw A. Animal model of human disease; multiple myeloma. *Am J Pathol* 1988, 132:593–597.

104. Fowler JA, Mundy GR, Lwin ST, Lynch CC, Edwards CM. A murine model of myeloma that allows genetic manipulation of the host microenvironment. *Dis Model Mech* 2009, 604–611:604–611.